HYDROKINETIC TURBINE POWER CONVERTER AND CONTROLLER SYSTEM DESIGN AND IMPLEMENTATION

by

Mofei Liu

A THESIS SUBMITTED IN PARTIAL FULFILLMENT OF
THE REQUIREMENTS FOR THE DEGREE OF

MASTER OF APPLIED SCIENCE

in

The Faculty of Graduate and Postdoctoral Studies

(Electrical and Computer Engineering)

THE UNIVERSITY OF BRITISH COLUMBIA
(Vancouver)

August 2014

Abstract

Due to environmental considerations and decline of fossil fuels, searching for the viable energy alternatives is a pressing need. In order to meet the energy demand globally, research into the renewable energy technologies must be pursued. Wind energy has emerged as the leader of new energy source, while other types of energy sources continue to be investigated. Hydrokinetic power as a potential opportunity to harvest energy is being explored recently. Because the hydrokinetic turbines are still in an early stage of development, study on the hydrokinetic system is an active topic of academic research. Although water speed is instable and unpredictable, the hydrokinetic system can still operate at the peak power point. For this reason, the power converter and rotor speed controller are the most important components in this study. In the first two chapters some background studies and some system components are introduced. In this project, the maximum power point tracking is realized by the hill-climb searching method and the lookup table method, plus the analysis and comparison of these two methods are presented. In terms of rotor speed controller design, the Field Oriented Control strategy is applied and discussed. The presented hydrokinetic system is a stand-alone system which throws excessive energy to a load resistor. In order to demonstrate the feasibility of the system, the hydrokinetic system model is simulated in the PSIM software. A number of cases are simulated with the PSIM model to validate the feasibility of this hydrokinetic system. Finally, the project objectives are achieved and some of the hardware is tested. Future work is still required, such as the bench testing with a real PMSG, a variable frequency drive, and the optimization of the maximum power point tracking method and rotor speed controller with the hardware test results.

Preface

The thesis is original, unpublished, independent work by the author, M. Liu.

As it is a collaboration project between UBC and Mavi Innovations Inc., the basic system design ideas and turbine characteristic information are owned and provided by Mavi Innovations Inc.

Table of Contents

List of Tables

List of Figures

List of Abbreviations

Direct Current—DC

Alternating Current—AC

Variable Frequency Drive—VFD

Induction Machine—IM

Permanent Magnet Synchronous Generator—PMSG

Tip Speed Ratio—TSR

Maximum Power Point Tracking—MPPT

Maximum Power Point—MPP

Power Regulation—PR

Hill-climb searching—HCS

Direct Torque Control—DTC

Field Oriented Control—FOC

Pulse Width Modulation—PWM

Space Vector Modulation—SVM

Insulated-Gate Bipolar Transistors—IGBTs

GW—Gigawatts

KW—Kilowatts

TW—Terawatts

Acknowledgements

I would like to express my deepest appreciation to all these who provide me the possibility to complete this thesis. A special gratitude I give to my supervisor Dr. William G. Dunford, who has been a tremendous mentor for me. Without his contribution in academic suggestions and support, this dissertation would not have been possible.

Then, I would like to thank Randal Clark, the director of engineering at Mavi Innovations Inc., who gave me a lot help and guidance on this project when I was working as an intern. And also the whole engineer team I worked with, Bill Rawlings, Voytek Klaptocz and Timothy Waung who are always patient with answering any questions and offering help.

Last but not least, I would like to acknowledge my families and my loved ones for supporting me spiritually through my life.

To my parents

Chapter 1 – Introduction

Because of the development of human society and modem technology, the demand for energy is growing year by year. More and more people are considering the depletion of the natural resources and its impacts on the environment. The conventional way of electrical power generation is by means of combustion of fossil fuels which always come with high pollution and will be exhausted in the future. For this reason, alternative sources of energy are required to solve the energy shortage problem as a long-term solution. In the search for the new source of energy, the renewable forms are the most desired. Therefore, the renewable energy, which is derived from natural processes that are replenished constantly, attracts a lot of attentions across the world. In order to protect our homeland for the next generation, a number of governments and institutions are calling for the investigation and the utilization of renewable power system to gradually improve the situation of dependence on fossil fuels.

From the world energy resources survey 2013 [2], the share of the renewable energy is 11% of the total energy supply by 2011, and this 11% does not include 2% large hydro energy (>10MW). After decades of research and development, the wind energy and solar energy have been already exploited all over the world. As a leading resource of the renewable energy in terms of harvesting technology, the total resource of wind energy is vast and estimated to be around one million GW for total land coverage. As mentioned in the survey, even if only 1% of this one million GW were utilized, with low load factors of wind plants (15-40%), this amount of energy would be sufficient to support the total worldwide capacity of all electricity generation in an operation day. The total wind energy capacity at the end of 2011 was over 238GW and the annual electricity generation is around 377TWh. As one of the most abundant energy resource, solar energy is available for use in anywhere. About 60% of the total energy emitted by the sun reaches the Earth's surface. Overall, there were 289 MWDC of solar photovoltaic (PV) capacity installed in Canada in 2011 representing over 335 gigawatt-hours (GWh) of power generation on an annual basis. [14] When comparing to mature technologies of wind power and solar power, the kinetic energy of water currents in rivers, oceans and estuaries is another form of sustainable and environmentally benign source, which is in the development, demonstration, and pilot phases of deployment and has not yet been commercialized. The power of tidal, river, and ocean

currents is sustainable, concentrated and tremendous, and the total tidal energy potential of the world is approximately 3 TW with 1 TW in accessible areas for installation of energy extracting devices. [3] Therefore, in order to investigate the feasibility for implementing hydrokinetic system, a study is presented in this paper.

1.1 Background of Hydrokinetic Power

Hydrokinetic technology is designed to produce the amount of electricity by capturing the energy from the flowing water in rivers, ocean tidal or estuaries. It converts the kinetic energy of water to the electrical energy in a clean and environment friendly way. The technologies developed to produce electrical energy from the kinetic power of water are called hydrokinetic energy conversion devices, which can be classified into wave energy converters or rotating devices by means of harnessing the kinetic energy. [4] Only the rotating device which is also called as hydrokinetic turbine will be discussed in this paper. As the most promising energy conversion method, hydrokinetic turbine inherits a substantial benefit from the vast technology experience in design, construction and installation of wind turbines gained in the last decades. The detailed introduction of the hydrokinetic turbines is presented in Chapter 2.

The hydrokinetic technologies are different from conventional hydropower facilities. Most of the hydroelectric plants require a large hydraulic head to power turbines for electricity generation. The hydraulic head can either be natural waterfall, or a dam in a riverbed which creates a reservoir. The water is controlled and released from the reservoir to create the required head to turn the hydro turbine. The traditional hydroelectric plants always have a large capacity for the electrical generation, but the costs and environmental impacts on constructing a dam are the main problem, so most of the hydrokinetic power systems are small-scale electrical generation sets, which operate in a “free flow” environment that does not require the damming or diversion of rivers. Free-flow deployment does not disrupt natural ecosystems or interfere with aquatic and marine life. Additionally, in some hydrokinetic energy deployment situations, hydrokinetic systems flexibly operated with multi-unit arrays, which would extract energy from flowing current in a similar way to a wind farm. The depth of the foundation of a hydrokinetic system and the spacing between systems are determined by the site conditions such as water depth and current flows. Like some other renewable energy sources, hydrokinetic power is variable, because the generation changes with the fluctuations in water speed. Unlike wind and solar

power, the variability of hydrokinetic power is highly predictable according to seasonal statistics. In the current development stage, the power generation capacity of remote hydrokinetic system does not generate much economic value for customers, so installing a transmission line is not affordable. Even though hydrokinetic turbine has lower environmental impact, it cannot replace the role of conventional hydro plants. In conclusion, as an alternative energy source, hydrokinetic systems are highly recommended for remote communities or coastal communities.

1.2 Research Objectives

The primary objective of this project is to design the power converter of the hydrokinetic power system that can be able to extract the maximum power from the flowing water. The hydrokinetic energy conversion device and the wind turbine system work in a similar way. When the water speed is large enough, a net positive power is produced by the hydrokinetic system. Because of the characteristic of the hydrokinetic turbine, there is only one optimal operation point producing the maximum power for each tip speed ratio, and the optimal operation point is determined by the water speed and shaft rotational speed. Because the water speed is uncontrollable, only the rotor speed can be adjusted to achieve the maximum power. Therefore, the appropriate power conversion algorithm and rotor speed controller are the key components with significant impact on system efficiency, reliability, function, capital cost and the total cost of ownership.

In order to complete the primary objective, several tasks are listed below.

1) Selection of system components, such as generator set, power electronics interface
2) Design of the Maximum power point tracking and power regulation methods
3) Design of the proper rotor speed controller
4) System integration and simulation model in the PSIM
5) Demonstration of hydrokinetic system by the case studies

Chapter 2 –Operation Principle and Mathematical Modeling of the Hydrokinetic System

In this chapter, the overall structure of the hydrokinetic system is given. The detailed introduction and analysis of each system components are described, such as the operation principle of different types of the hydro turbine, types of the generator and also types of power electronics interface. At last, the mathematical models of the turbine and the generator are presented.

2.1 The Overview Structure of the Hydrokinetic System

The hydrokinetic system is an electrical power generation system which extracts energy from the flowing water and produces the quality electricity to the utility grid or remote communities. Hydro energy is available in many forms, which are potential energy from high heads of water retained in dams, kinetic energy from current flow in rivers and tidal barrages, and kinetic energy also from the movement of waves on relatively static water masses. The system described in this study is a small-scale hydrokinetic system that is always deployed in the river or tidal environment. For those with riverside homes or live-on boats, small water generators (low head hydro power) are the most reliable source of renewable energy. Because the variation of the water speed is similar to the wind speed, the system structure and operation principles are similar to the wind power system. Therefore, the overall structure of the hydrokinetic power system is illuminated in figure 2-1.

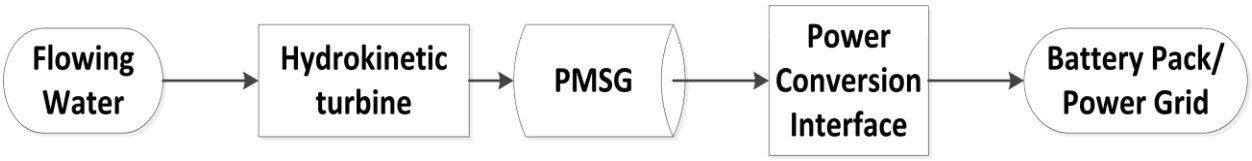

Figure 2-1 Structure of the hydrokinetic system

As shown in figure 2-1, the system consists of a hydrokinetic turbine, generator (PMSG), power conversion interface and battery/grid. When the turbine is merged into the water, the flowing current turns the turbine, and the coupled generator rotor will spin along with the turbine shaft. If an induction machine is used as the generator, a gear is required between the generator and the turbine to produce the corresponding frequency during the lower water speed, but nevertheless,

the permanent magnet synchronous generator can connect to the hydrokinetic turbine directly. The output power is controlled and converted by the power conversion interface. For a grid-connected system, an inverter connects to the DC bus to convert the DC power to the AC power and then exports such power to the power grid. For a stand-alone system, a load resistor and a battery pack are attached to the DC bus. The load resistor is used to dissipate the extra power produced by the system when the battery is fully charged. The suitable load resistor should be able to consume the power on the DC bus without being over-heated and burnt off. In the real system, the commercial product – Variable Frequency Drive (VFD) is used to realize the function of power conversion interface. Moreover, the battery pack is also used to power up the VFD, generator and some other instruments of the system.

2.2 Classification of Hydrokinetic Turbines

Hydro turbine like a windmill is a rotary engine operating in the water, and it converts hydrokinetic energy to mechanical energy. Unlike the turbines used in the large hydro dam, which produce large amounts of energy from potential energy of waterfall, the turbines used in the low head power applications are different. As the definition, the theory of operation is described as the moving water is directed onto the blades of a turbine runner and creating a force on the blades. Due to the spinning runner, the force acts through a distance and energy is transferred from the water flow to the turbine.

Based on the development of wind turbine technologies, many hydrokinetic energy devices are created. The classification of hydrokinetic turbines has been proposed by T. J. Hall. [16] A chart of turbine classification is shown in figure 2-2 provided by [17]. Generally, almost all the low head hydro turbines are classified into two types: axial flow and cross flow (shown in Figure 2-3 & 2-4), and further classification is determined by the direction of the fluid flow relative to the rotational axis.

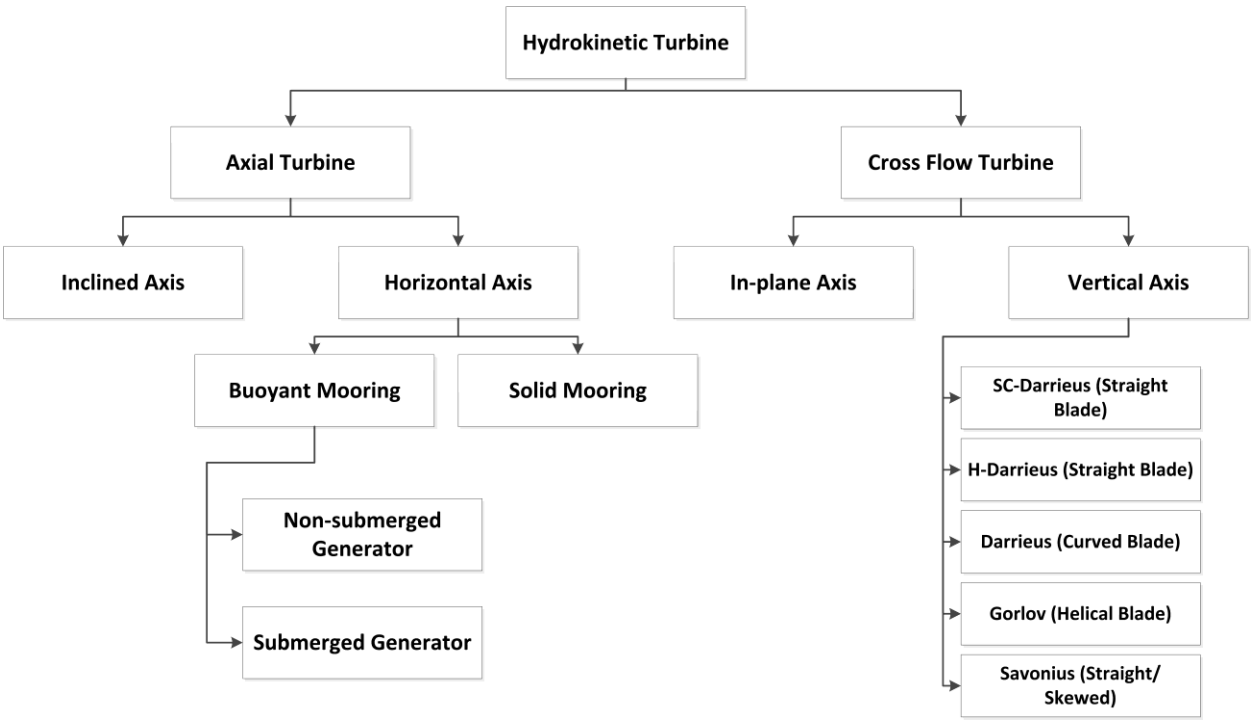

Figure 2-2 Classification of hydrokinetic turbines

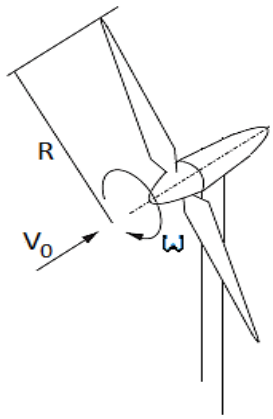

Figure 2-3 Axial flow turbine [16]

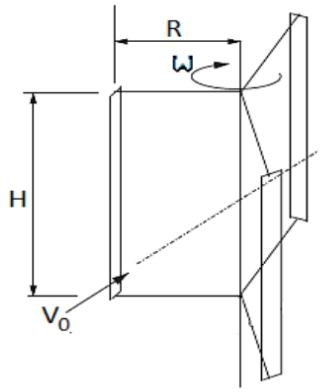

Figure 2-4 Cross flow turbine [16]

The axial turbine is given such a name because the flow direction is parallel to the axis of rotation, and its horizontal axial counterpart, which is called as horizontal axis turbine is commonly used in the wind industry. Over decades of research and implementation, the axial turbine technology has been fully developed for the renewable energy applications. This type of turbine is mostly used exclusively in the wind power system except for some small-scale residential applications. Another type of turbines is called cross flow turbines which have their rotation axis perpendicular to the flowing water and mostly appear as cylindrical rotating structures. Cross flow turbines are less efficient than axial flow turbines, however, cross flow

turbines have many potential advantages for marine applications. Firstly, the cylindrical shape of cross flow turbines allows themselves to be easily stacked and arranged in an array within limited space. The efficiency of each individual cross flow turbine can be increased in the power farm. In addition, the stacking of cross flow turbines is allowed to share a common electric converter, and this technique reduces equipment and maintenance costs as a very important advantage in the hydrokinetic application. As a disadvantage, axial flow turbines typically reach higher tip speeds, making them more prone to cavitation, which reduce the efficiency and create surface damage. Comparing to the axial turbines, the cross flow turbines can rotate undirectionally even with bi-directional current flow. In this project, the cross flow hydrokinetic turbine is employed. Because Mavi designs hydrokinetic turbine, this part is an introduction which would not be the contribution of this thesis.

2.3 Types of System Generator

Generators are used to convert mechanical energy to electrical energy. A number of generators can be connected to the shaft of the hydrokinetic turbine, such as DC generators (Dynamo), AC synchronous generators (permanent magnet, field excitation) and AC asynchronous generators (induction generator). The power range, rotor speed, types of the load, maintenance and cost are the considerations for selecting the proper generator of the hydrokinetic system.

2.3.1 DC generator

DC generator, also named as Dynamo, is an electrical generator that produces direct current. Due to the high maintenance of the commutator and oversize issue, DC generators are rarely applied in the large power generation systems or the renewable energy applications. Another disadvantage of the DC generator is that the inverter devices used with DC generator to convert DC voltage to the AC voltage are not efficient and economy. Therefore, DC generator is not appropriate for the hydrokinetic system.

2.3.2 Induction generator

By comparing with all types of generators, both induction machines and synchronous generators are popular used because of their numerous advantages for wind and hydrokinetic applications. Induction generators (asynchronous generators) are widely and commercially applied in the electrical power generation system because of their availability and low costs. The induction machine can be operated at the generator model or the motor model. When the shaft rotating

speed is lower than the machine synchronous speed, the machine works as a motor. In order to operate the machine as a generator, the rotor should be rotating faster than the synchronous speed. Because of the ability of producing power at variable speed, induction machines are often used in wind power or some micro hydro applications. Unlike the synchronous generator, induction machines are load-dependent and cannot be used alone for grid frequency control. The main disadvantage of using an induction machine as the generator is that a gearbox will be introduced in the turbine system. Because the water velocity is too low to match the synchronous speed of the machine, the gearbox is required to speed up the rotor speed, however, a gearbox system can provide machine noise, losses and increase the cost of the system for frequent maintenance. In addition, the gearbox also makes the hydrokinetic system more complicated with less reliability.

2.3.3 Permanent magnet synchronous generator (PMSG)

As the majority source of commercial electrical energy, synchronous generators are commonly used to convert the mechanical energy into the electrical power. Permanent Magnet Synchronous Generator (PMSG) is a synchronous generator whose excitation field is provided by the permanent magnet. Permanent magnets can be used to replace the excitation winding of synchronous machines because of the magnet price reduction and magnetic material characteristic improvement. [7] In the past decades, PMSG has become more and more popular because of its higher efficiency and power density. In addition, the permanent magnet generator technology is advancing with the low maintenance and high reliability for long-term application and giving a reduction in operational cost. The multipole PMSG can connect to the turbine shaft directly at a low rotating speed without a gearbox. This is a solution for small-scale system with variable wind speed as well as variable water speed. Moreover, due to the large number of pole pairs, the permanent magnet structure enables a mass reduction in the stator yoke and rotor back iron. As a result, the development of the low speed synchronous generators with the permanent magnet excitation field has been received high attention all over the world. [8] Another advantage of the synchronous generator is that the synchronous generator ensures the frequency of the output voltage is proportional to the rotor speed, and this is important principle for maximum power point tracking method.

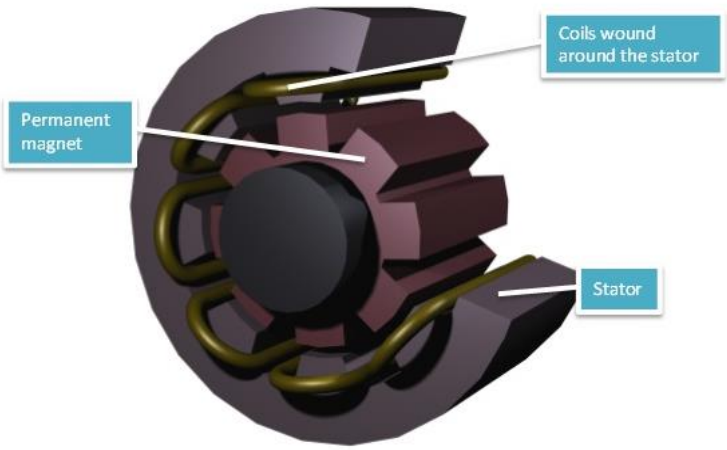

Figure 2-5 Structure of PMSG [9]

The structure of the surface mounted magnet PMSG is shown in figure 2-5. It is composed of a rotor having a permanent magnet mounted on the surface and a stator with a stationary armature which is electrically connected to the load. By comparing with the induction machine, there is no current flowing through the rotor. Therefore, the copper loss in the PMSG can be considered as half of the induction machine. Because the magnetic field is provided by the permanent magnet, there is no need to have a DC supply externally for excitation or a slip ring or contact brushes like other generators, however, PMSGs have a number of drawbacks which restrict the development of PMSGs. Because of the high price of large permanent magnet, it is not economic to use the PMSG in the commercial large-scale generation system. Additionally, the flux density of the high performance magnet is limited. Another issue needs to be considered is the risk of demagnetization of magnets due to the temperature rise. Because the air gap flux is not controllable, the output voltage of the generator cannot be regulated easily. Therefore, a converter is required to control the voltage of the PMSG.

In this project, a direct drive PMSG is selected to play the role of the generator of the hydrokinetic system. The data sheet of the PMSG parameters, which will be used in the bench testing, is shown in Appendix A.

2.4 Hydrokinetic Power Conversion System

The power conversion strategy is an important part in the hydrokinetic system, and it determines the efficiency, reliability and economy of the hydrokinetic system. For the stand-alone system, the power conversion system always contains a rectifier to convert the 3-phase AC output voltage to the DC voltage, a DC bus, a load resistor to dissipate the extra power, and a battery pack to be used as energy storage. The grid-connected system uses a DC/AC inverter (Active Front End) connected between the DC bus and the power grid to replace the load resistor and battery pack. A series of power conversion strategies in the hydrokinetic turbine are described as below.

In the stand-alone system, the first power conversion strategy is presented in figure 2-6.

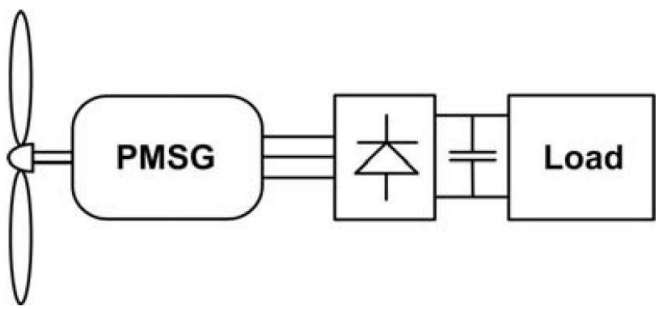

Figure 2-6 Strategy with a diode bridge [13]

In figure 2-6, a conventional diode rectifier is used to convert the 3-phase AC voltage to the DC voltage directly without any control strategies. The battery pack or load resistor connects to the DC bus. The advantage of this strategy is simplicity and low costs, but this strategy develops high harmonic distortion in the output current of the generator, and the harmonic components may cause upsets in the generator, such as machine efficiency reduction, heating issue. Furthermore, the variable speed control is not available in this configuration. Thus, this conversion strategy is not recommended for the hydrokinetic system.

In order to overcome these problems, a more popular strategy is shown in figure 2-7. A boost DC/DC converter is employed between the diode rectifier and DC bus to control the voltage level of DC bus and realize the variable rotor speed control by adjusting the duty cycle of the DC/DC converter. In order to reduce the harmonic distortion produced by the power electronics converters, the line reactors are added. The advantage of this strategy is that only one switch in

the circuit will be controlled, which means the system is simple and also the switching losses are low. Even though the diode bridge rectifier provides high reliability and low costs, it is difficult to achieve the optimal current control such as loss-minimization control and flux-weakening control for PMSG and a serious stator harmonic current is introduced, and it may lead to significant electromagnetic torque ripple.

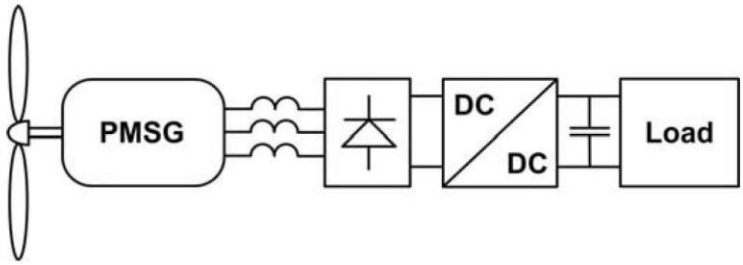

Figure 2-7 Strategy with DC/DC converter [13]

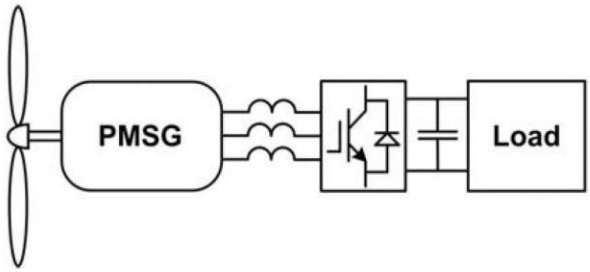

Figure 2-8 Strategy with 3-phase PWM rectifier [13]

Figure 2-8 presents a more advanced strategy that a 3-phase PWM rectifier is introduced into the conversion system to replace the conventional diode rectifier. The rectifier controls the d-q axis currents by the PWM signal generated from the rotor speed controller. This strategy cannot only realize the variable rotor speed control of the PMSG but also the control of electromagnetic torque and active and reactive power. Even though six switches make the control scheme complicated, it does provide good control flexibility. In addition, using IGBTs as the switches reduces the switching losses and makes the system working in a wide range. Another advantage of this rectifier is bi-directional operation, which means the power can flow back to the generator from the battery pack to start up the turbine system.

For the grid-connected system, a PWM inverter is attached to the DC bus to convert the DC voltage to the 3-phase AC voltage and import the power to the grid. This configuration is called as back-to-back PWM converter. For the grid-side inverter, the controller can realize the function

of power factor correction and DC bus voltage level control. In this project, the strategy with 3-phase PWM rectifier and IGBT switches is utilized as the power conversion system.

2.5 Selection of RLC Filter and Line Reactor

A harmonic filter is used to eliminate the harmonic distortion, and it is built with a capacitor, an inductor, and a resistor. Each harmonic filter could contain many such elements, each of which is used to deflect harmonics of a specific frequency. The cutoff frequency of the low pass filter is defined as:

$$f_c = \frac{1}{2 * \pi\sqrt{C * L}} \tag{2.1}$$

where C is the capacitance and L is the inductance.

From the PMSG parameters (Appendix A), the maximum rotor speed of the generator is 130 RPM and the number of pole pairs is 24, so the output frequency is 52Hz which is derived as:

$$f = \frac{RMP * Pp}{60} \tag{2.2}$$

where RPM is the shaft speed and Pp is the number of pole pairs.

In order to eliminate the harmonic distortion in the output power, the cut off frequency should close to the specific frequency. For this reason, the RLC filter (R=0. 001, C=0. 75mF, L=8. 5mH) is applied as the low pass filter, which is located between the PMSG and the rectifier, and the cutoff frequency is 63Hz. These values are used in the RLC filter of the simulation model in Chapter 4.

When using the VFD in the real system, a line reactor is used. It helps VFD from input power line disturbances which could cause damages to the drive, and the line reactor also reduces the harmonic that the VFD generated back onto the line. As [12] mentioned a higher inductance of the filter leads to lower current total harmonic distortions value, but the power capacity of the inverter decreases.

2.6 The Mathematical Model of Hydrokinetic Turbine

The hydrokinetic turbine or hydrokinetic conversion device (HCD) is a mechanism that converts hydrokinetic energy to the mechanical energy. Mechanically, the turbine is influenced by the

flowing water, and opposing torque from the generator. The difference between the torque produced from the turbine and counter torque from the generator leads the acceleration of the rotor until they balance each other at a certain shaft speed. The amount of the inertia determines the acceleration rate. The hydrokinetic turbine has a similar dependence on water velocity as the wind turbine on wind speed. In general, most of the principles and equations are similar to the wind turbine theory. The amount of kinetic energy can be described as [34]:

$$P_t = \frac{1}{2} C_p(\lambda) \rho \mathrm{A}_t V_w^3 \tag{2.3}$$

where C_p is the power coefficient of the hydrokinetic turbine, λ is the Tip Speed Ratio, $\mathrm{A}_t$is the cross sectional area of the turbine through water flows, $V_w$is the water velocity.

The Tip Speed Ratio (TSR) can be expressed with the turbine radius R_t, turbine rotational speed ω_t and water velocity V_w as [34]:

$$\lambda = \frac{R_t \omega_t}{V_w} \tag{2.4}$$

The power coefficient C_p represents the amount of kinetic power that can be extracted from the flowing water. It is a function of TSR and pitch angle β. This function is given in terms of a curve from the turbine manufacturer since it characterizes the efficiency of the water turbine, which means the shape of the power coefficient curve is determined by the turbine. If this curve is not provided, it can be obtained from the field-testing. In this hydrokinetic system the pitch angle of the turbine is assumed constant and the impact of the pitch angle is negligible, so the power coefficient depends on the TSR only.

The output power from the turbine can be expressed:

$$P_t = \omega_t T_t \tag{2.5}$$

Therefore, the torque produced by the hydrokinetic turbine is given [34]:

$$T_t = \frac{P_t}{\omega_t} = \frac{1}{2} C_t(\lambda) \rho \mathrm{A}_t R_t V_w^2 \tag{2.6}$$

$$\lambda = \frac{C_p(\lambda)}{C_t(\lambda)} \Longrightarrow C_p = \frac{R_t \omega_t}{V_w} C_t \tag{2.7}$$

where $C_t(\lambda)$ is torque coefficient of the turbine. Same as the power coefficient, torque coefficient is determined by the design of the turbine. As a result, the torque coefficient corresponds to a particular rotor speed and the shape of the torque curve is similar to the power curve. The curve

of the power coefficient C_p vs. TSR and the curve of the torque coefficient C_t vs. TSR will be described in Chapter 4.

As shown in equation 2.4, for constant water speed there is only one optimum rotor speed to obtain the maximum power. The power curves corresponding to each water speed will be shown in Chapter 3. Consequently, in order to obtain maximum power from the hydrokinetic turbine generator system, it is necessary to drive the turbine at the optimal rotor speed for a particular water speed. This is the basic principle of Maximum Power Point Tacking (MPPT), which will be also described in the next chapter.

2.7 The Mathematical Model of Direct Drive PMSG

Due to the complex structure and technology of the PMSG, it is necessary to simplify the system equations for better understanding and analysis. A number of equations are given in this section, and the rotating transformation is applied to transfer three phase variables of generator to d-q-0 frame, and it is helpful for defining a dynamic model of generator system and designing generator control system. The PMSG is coupled with hydrokinetic turbine directly, so the rotating speed changes with the water speed. As it is known as synchronous generator, f the frequency of the induced voltage in the stator is directly proportional to the rotor speed RPM. Therefore, the constant of proportionality is represented by equation 2.2.

The synchronous generator modeling is usually based on assumptions on:

1) The stator windings are balanced and air gap flux is sinusoidal.
2) Saturation and parameter changes are neglected.
3) The effect of stator slots on the rotor inductance with rotor positions is ignorable.
4) Hysteresis losses and eddy current losses are neglected.

According to these assumptions, the dynamic model of the PMSG can be represented in the d-q-0 reference frame, and the q-axis is 90 degrees ahead of d-axis according to the direction of rotation.

2.7.1 Rotating (direct-quadrature-zero) transformation [10]

The direct-quadrature-zero (d-q-0) transformation is a transformation of coordinates from the three-phase stationary coordinate system (a-b-c) to the rotating coordinate system (d-q-0). It

defines a new set of stator variables such as currents, voltages or flux linkages in terms of actual winding variables. The new quantities are obtained from the projection of the actual variables on three axes; one along the direct axis of the field winding, called the direct axis (d-axis); a second along the neutral axis of the field winding, called the quadrature axis (q-axis); and a third on a stationary axis (0-axis). This transformation can be made from two steps [11]:

(1) **Clarke transformation** which outputs a two coordinate time variant system attach to the machine stator. It is a transformation from the three-phase stationary coordinate system to the stationary α-β coordinate system. The Clarke transformation is used to transform the three-phase current quantities i_a, i_b , and i_c into two-phase orthogonal stator axis currents $i_{s\alpha}$ and $i_{s\beta}$.

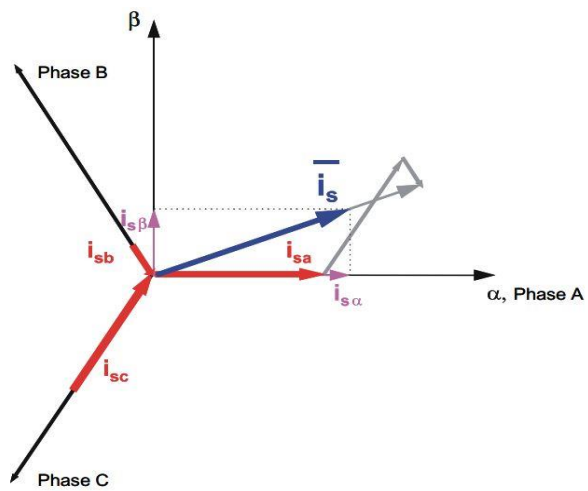

Figure 2-9 Clarke transformation

(2) **Park transformation** is a transformation that outputs a two coordinate time invariant system, oriented with its real axis d in the direction of magnetic flux orientation. It is a transformation from α-β stationary coordinate system into the d-q rotating system. The two currents in the fixed coordinate stator phase $i_{s\alpha}$ and $i_{s\beta}$ are transformed into the d-q rotating frame as i_{sd} and i_{sq} current components using park transformation.

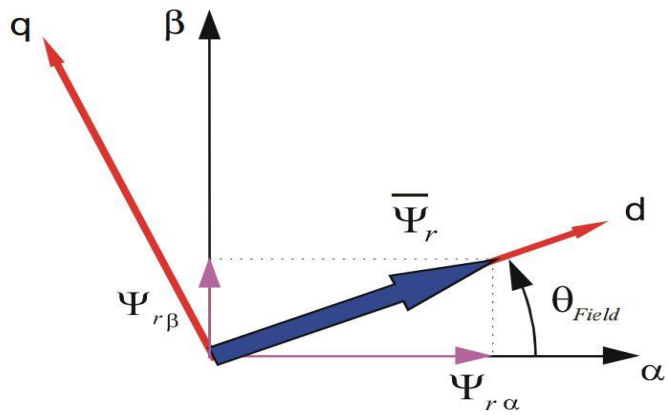

Figure 2-10 Park transformation

The d-q-0 transformation is defined as follow in matrix form [10]:

$$x_{dq0} = Kx_{abc} = \sqrt{\frac{2}{3}}\begin{bmatrix} \cos(\theta) & \cos(\theta - \frac{2\pi}{3}) & \cos(\theta + \frac{2\pi}{3}) \\ -\sin(\theta) & -\sin(\theta - \frac{2\pi}{3}) & -\sin(\theta + \frac{2\pi}{3}) \\ \frac{\sqrt{2}}{2} & \frac{\sqrt{2}}{2} & \frac{\sqrt{2}}{2} \end{bmatrix}\begin{bmatrix} x_a \\ x_b \\ x_c \end{bmatrix} \tag{2.8}$$

Where $\theta = \omega t + \varphi_A$ is the angle between the rotating and fixed coordinate system at time t and φ_A is an initial phase shift.

The inverse transformation from the dq0 frame to be three phases ABC frame is:

$$x_{abc} = K^{-1}x_{dq0} = \sqrt{\frac{2}{3}}\begin{bmatrix} \cos(\theta) & -\sin(\theta) & \frac{\sqrt{2}}{2} \\ \cos(\theta - \frac{2\pi}{3}) & -\sin(\theta - \frac{2\pi}{3}) & \frac{\sqrt{2}}{2} \\ \cos(\theta + \frac{2\pi}{3}) & -\sin(\theta + \frac{2\pi}{3}) & \frac{\sqrt{2}}{2} \end{bmatrix}\begin{bmatrix} x_d \\ x_q \\ x_0 \end{bmatrix} \tag{2.9}$$

The synchronous frame can be aligned to rotate with the voltage or with the current. Noted that in the d-q frame the zero-component is $x_0 = \frac{1}{3}(x_a + x_b + x_c)$. Therefore, on system with no neutral connection, the 0-component will be omitted.

The instantaneous active and reactive power from a set of two-phase (d-q) voltages and currents are [35]:

$$P = u_d i_d + u_q i_q \tag{2.10}$$

$$Q = u_q i_d - u_d i_q \tag{2.11}$$

When the synchronous frame is aligned to voltage, the quadrature component: $u_q = 0$. Therefore, the power equations reduce to:

$$P = u_d i_d \tag{2.12}$$

$$Q = -u_d i_d \tag{2.13}$$

In conclusion, for three-phase system with no neutral connection, the d-q-0 transformation can reduce three phase AC quantities into two DC quantities, and the 0-component is zero. The DC quantities facilitate easier filtering and controlling. In addition, active and reactive power can be controlled independently by controlling the d and q components.

The stator voltage of PMSG in d-axis and q-axis are given below [18]:

$$u_{sd} = R_s i_{sd} + L_d \frac{di_{sd}}{dt} - \omega_e L_q i_{sq} \tag{2.14}$$

$$u_{sq} = R_s i_{sq} + L_q \frac{di_{sq}}{dt} + \omega_e \lambda_m + \omega_e L_d i_{sd} \tag{2.15}$$

where u_{sd} and $u_{sq}$are the d-axis stator voltage and q-axis stator voltage respectively, R_s is the stator resistance, L_d and L_q are the inductances of the PMSG in the d-q axis, λ_m is the magnetic flux and the reference flux is synchronized with the magnetic flux.

The electrical angular speed (Rad/s) can be defined as:

$$\omega_e = Pp * \omega_m \tag{2.16}$$

and $\omega_m$is the mechanical angular speed of the generator, Pp is the number of pole pairs.

The expression of the electromagnetic torque of the generator is given by [18]:

$$T_e = \frac{3}{2} Pp[(L_q - L_d) i_{sq} i_{sd} + \lambda_m i_{sq}] \tag{2.17}$$

For simplify analysis, the inductive components of the surface mounted PMSG in the direct and quadrature axis are regarded as identical ($L_q = L_d = 10.9mH$). So the electromagnetic torque can be expressed as:

$$T_e = \frac{3}{2} Pp(\lambda_m i_{sq}) \tag{2.18}$$

Then the mechanical equation of the rotating generator including the angular rotor speed is given by the following equation [18]:

$$J_g \frac{d\omega_m}{dt} = T_e - B\omega_m - T_L \tag{2.19}$$

where $J_g$is the equivalent inertia of the PMSG and B is the fiction coefficient of the PMSG.

Chapter 3 – Power Converter and Controller Design of Hydrokinetic System

The main idea of this chapter is to describe the detailed design process and analysis for the power converter and rotor speed controller in the hydrokinetic system. These two items are the main points to realize the MPPT of the system. The simulation models and the feasibility analysis are described in the Chapter 4.

3.1 The Power Conversion Strategies of Hydrokinetic System

Because the velocity of flowing water is variable and erratic, developing reliable and efficient methods to track the optimal operation point of the hydrokinetic system is necessary to extract the maximum available power from water.

3.1.1 System operation status

In order to produce the maximum power output and protect the system, the operation of the hydrokinetic system can be divided into several operating phases, as shown in figure 3-1 below:

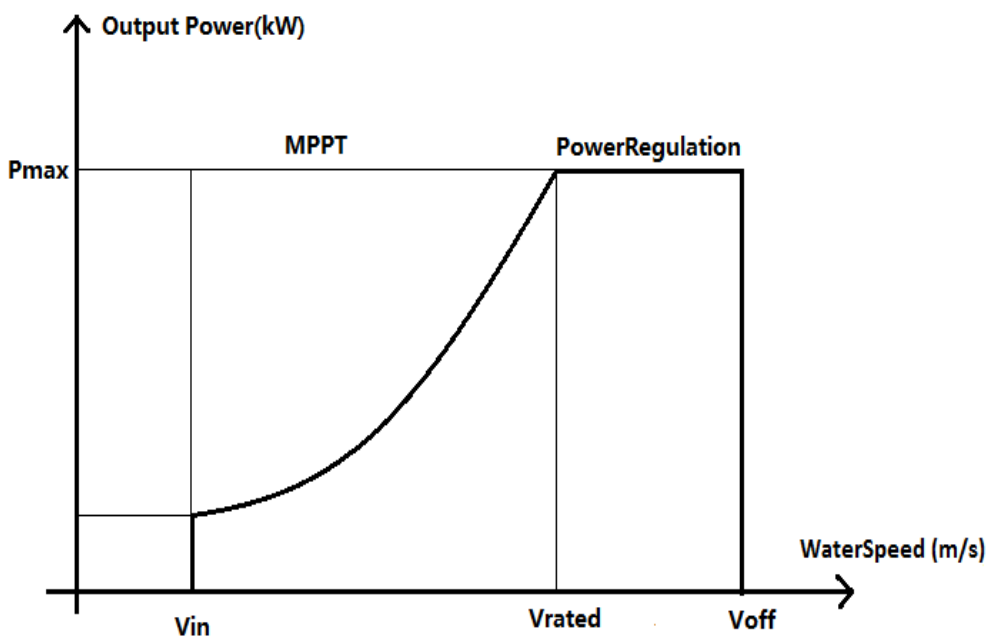

Figure 3-1 System operation status

As revealed in figure 3-1, the system operation status can be divided into four regions:

1) **Cut-in Region or Dead Zone**. In this region, the water velocity is so low that water cannot produce sufficient torque to drive up the hydrokinetic turbine to produce power. In this case, if the turbine is rotating, the hydrokinetic system would drain power from the grid or from the battery pack. In bi-directional system, the battery pack is supposed to support driving the sensors, microcontroller and VFD. During this period, the hydrokinetic system is turned off and waiting for the water speed to increase to the cut-in speed before moving to the next region.
2) **Maximum Power Point Tracking (MPPT) Region.** When the water speed reaches to the cut-in speed, which means the water is capable to drive up the system and a net positive power is generated. The system will start up and need a MPPT in this significant phase. The MPPT is mostly required as the hydrokinetic system is trying to maximize output power during an accelerating or decelerating flowing water. The MPPT starts at the cut-in speed (1.5m/s) and ends at the rated operation speed (3m/s). During this water speed range, the rotor speed controller will operate so that the turbine and rotor of the generator will rotate at the optimal speed for a particular water speed in order to obtain the maximum power. A rotor speed controller provides d-q current control and outer loop speed control for the reference speed command from the MPPT/Power regulation block. The strategies and methods of MPPT will be discussed in the next section.
3) **The Power Regulation Region.** This is a region that requires hydrokinetic system to maintain the output power within its operating limits (generator rated power) by reducing the rotor speed to a lower value than the optimal speed. For regulating the system to the specific maximum power, turbine power must be lower than the generator rated power. Once the actual water speed passes the rated water speed of the hydrokinetic system, the turbine power should be regulated. The rated operation rotor speed (120RPM at water speed 3m/s) is the point that the operation status of the hydrokinetic system switches from MPPT region to the Power regulation region. Furthermore, the rated power, the rated water speed and the rated rotor speed are also obtained at this point. For example, when the actual water speed is higher than the rated water velocity (3m/s), the maximum output power at the optimal rotor speed is higher than the rated output power, and exceeds the limit of the hydrokinetic system. In order to protect the system and also produce the maximum available power, the operation point is controlled at the left hand

side of the optimal operation point and the output power is maintained at the rated output power. Therefore, as shown in figure 3-1, the output power line should be flat in this region.

4) **Cut-out Region.** Due to the operating limits, a microcontroller is implemented to control a mechanical brake which stops the turbine when the actual water speed exceeds the cut-out water speed (4.5m/s). The turbine remains off until the water speed decreases to the power regulation region. The reason for not using the power regulation strategy for the higher water speed is that the turbine can produce higher torque ripple which can cause serious damages on the hydrokinetic system. Therefore, it is necessary to shut down the turbine when the water speed is very high.

Under the river circumstance, the water velocity varies slowly in a small range, so the hydrokinetic system will operate in MPPT region and Power regulation region most of the time, however, under the ocean tidal circumstance, the water velocity varies periodically, so the hydrokinetic system will be shut down for 4 or 3 times in a day. For the river application, water speed sensors or predictive methods are needed to determine the phase of operation of the hydrokinetic system. A cost-effective water speed sensor with an acceptable tolerance in accuracy can be implemented to monitor water speed, because the information for cut-in speed and cut-off speed will be sufficient for the system's operation. In another way, the predictive method for determining the system operation status is to turn on the system every 5 minutes to check if the water condition is suitable to drive the system up when the turbine is shut down. The predictive method can eliminate the delay introduced by the water speed sensor, but it may cause the system to suffer a large torque for initiating operation.

3.1.2 Literature review of the MPPT and power regulation techniques

The general idea of the MPPT strategy is to find the optimal rotor speed for the corresponding water speed, to produce the maximum available output power of the hydrokinetic turbine. Various sensors can be applied as input to enhance the performance of the MPPT of a hydrokinetic system, such as speed sensor for measuring the instantaneous water velocity, generator output voltage sensor, current sensor , and the output of the MPPT is the reference speed (optimal speed) for the rotor of the hydrokinetic system. To demonstrate various techniques for MPPT algorithm, a literature review of the currently MPPT techniques is given below.

In [28], G. Moor and H. Beukes proposed a strategy that is to make use of a pre-determined lookup table or an equation to describe the loading required to achieve the maximum power point. The lookup table is a curve describing the relationship between the wind speed and the reference rotation speed to keep the TSR at the optimal value. The TSR characterizes the aerodynamic efficiency of wind turbine and there is only one TSR value for the maximum power. This curve should be pre-programmed into the controller, which is calculated from an expected power profile or physically measured during preliminary practical testing of wind turbines. There are two methods to obtain the quantity of the wind speed. One is measuring the wind speed with an anemometer which is precise but expensive instrument for small turbines. For cost-effectiveness, calculating the wind speed from the available electrical parameters at the generator's terminal can be implemented as an alternative. The advantage of the lookup table strategy is fast determination for the optimal point and the simplicity of the turbine power system, because all of the parameters are predetermined with the characteristics of the turbine and no delay is introduced into the system. On the other hand, the disadvantage of this strategy is that a lookup table is only customized for a particular turbine.

Another MPPT strategy proposed by E. Koutroulis and K. Kalaitzakis [29] is presented by adjusting the duty cycle of the buck type DC/DC converter based on the comparison of the output power using measurements of wind generator's output voltage and current. In his paper, the system is a stand-alone system and it consists of a rectifier, a DC/DC converter and a battery pack. A microcontroller is applied to control the converter and the battery charging switches. The difference between lookup table method and this duty-cycle method is that Koutroulis and Kalaitzakis proposed a relationship between the variation in the output power and the converter duty cycle, and this relationship includes a single extreme point coinciding for a wind power characteristic curve. Thus, the algorithm determines the adjustment on the change in power with respect to the duty cycle. The converter duty cycle adjustment accords to the control method of the hill-climb searching. In order to reduce the impact of sensor accuracy of the generator power, the control method is based on the increment of power measurement rather than absolute power measurement. The advantage of this algorithm is that there is no requirement for the costly wind speed anemometer and the knowledge of wind turbine optimal power characteristic. But the

drawback is that the adjusting process introduces the lagging of the system, which means the desired optimal power point would never be reached in time.

R. Datta and V.T. Ranganathan [31] use hill-climb searching as a method of tracking peak power points in their wind turbine system and this method is independent of turbine parameters and air density. The proposed algorithm searches peak power by adjusting the reference speed in the desired direction. Based on the variation of the magnitude and direction of the active output power, the generator is controlled in the speed mode with the reference speed being dynamically modified. The peak power points in the $P - \omega$ curve correspond to $\frac{dP}{d\omega} = 0$. As described in [31], the generator speed and output power are sampled with a small interval of time. When the wind speed is steady, there is no change in the output power, then the differential value is zero, thus there is no action for the reference speed. When there is a step change in the wind speed, since the turbine speed cannot change instantaneously, there will be a corresponding change in power output. For this reason, a positive power change causes an increment on the speed command and vise versa, and the size of step change is made proportional to the change of power. For further adjustments, the speed reference direction is determined by both of the change in power and previous speed reference direction. This algorithm definitely has the advantage of independent turbine parameters, so it can be employed to any particular turbine system without parameter determinations. However, this algorithm still owns some drawbacks. For example, the searching procedure always takes time to find the optimal point and the relocation continuously happens when the operation is close to the optimal point.

In summary, the MPPT strategies can be divided into two categories: one is customized method with pre-determined system parameters and the other is independent one with power searching process. Such as [29] and [31], they do not require any information of the turbine characteristics and can be applied to various turbines. These techniques, however, would be slower than the look-up table method in [28]. Even though the look-up table method is efficient and reliable, prior knowledge of the particular turbine system or physical testing is required. In order to avoid the delay problem in hill-climb searching method, [32] introduces an intelligent memory algorithm, which allows the algorithm to be more efficient over time and the optimal points can be stored for later use. Another point is that techniques that employ sensors are relatively

expensive, but they perform well with water speed variations, particularly when the control system responds quickly. The water speeds evaluation may produce the wrong value when there is a transient variation in the water velocity. Thus, for real system design, a number of factors should be taken into account to balance the profit.

3.1.3 Proposed power conversion algorithm in the hydrokinetic system

The proposed power conversion algorithm used in this hydrokinetic system includes two modes: MPPT mode is realized through the hill-climb searching method to extract the maximum available power from the turbine by commanding the rotor to operate at a particular speed. Another one is Power regulation which is obtained by basic perturbation and observation method in order to maintain the output power below the system limitation when the water speed is higher than the rated speed.

The operation principle of proposed algorithm is similar to the standard wind power hill-climb searching strategy, the algorithm searches for the peak power by varying the reference rotor speed in the desired direction. The input to the algorithm block is turbine output power, which is measured from system or given by the product of torque and speed of the turbine. Since the power losses in the system are small, the line power is close to the turbine output power. The output from the block is the rotor speed command for the corresponding water velocity. The power and speed is sampled at a constant time interval (Time step=5e-5s). This algorithm is coded in the C which is shown in Appendix B. Figure 3-2 is presenting the flowchart of the code logic.

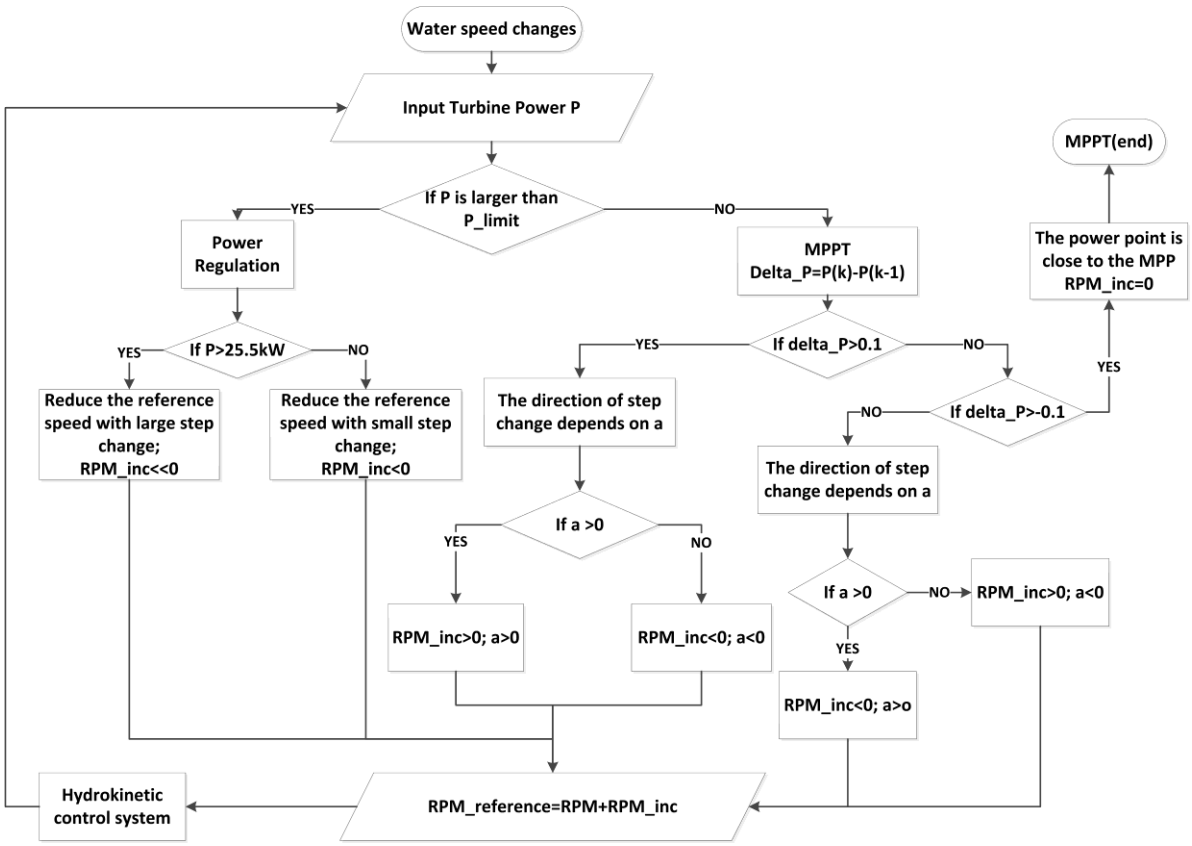

Figure 3-2 Flowchart of MPPT/Power regulation algorithm

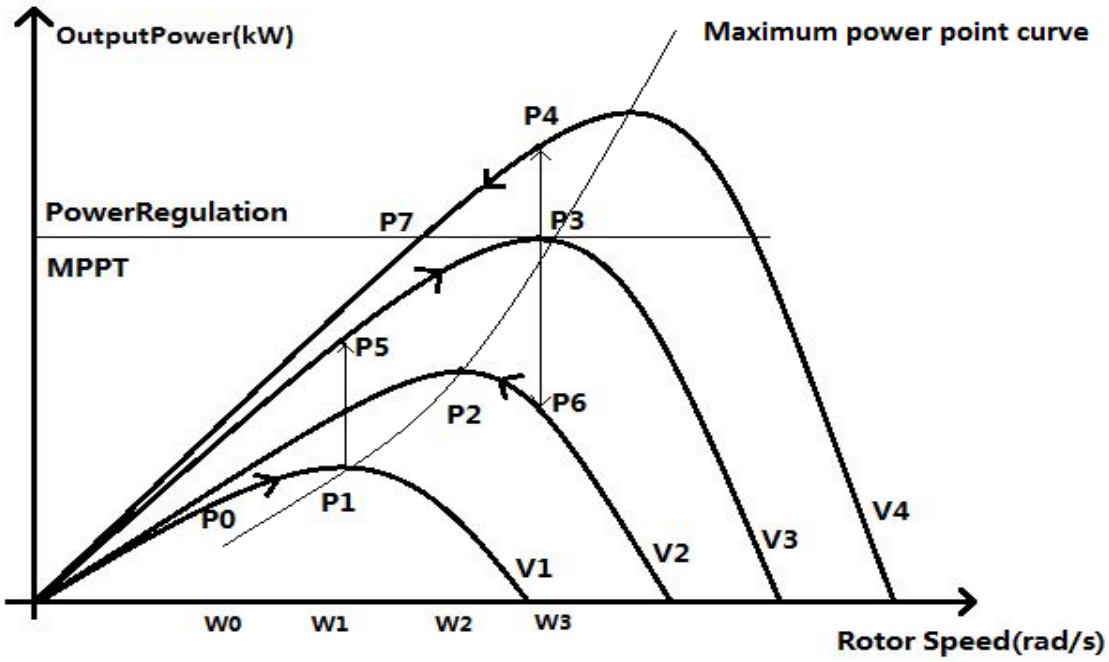

Figure 3-3 Power characteristic of turbine vs. rotor speed

The procedure of this proposed algorithm can be explained with the $P - \omega$ curve shown in figure 3-3. From the figure, it can be seen that y-axis represents the output power of the turbine and x-axis represents the rotor speed. Based on the turbine power characteristic there is only one maximum power point on each $P - \omega$ curve for a particular water velocity. Thus there are four power curves corresponding to four water speeds ($v_1 < v_2 < v_3 < v_4$). The pitch angle is assumed to be fixed for the hydrokinetic system. If the present water speed is v_1 and the turbine is rotating at the speed of ω_0, a power of P_0 can be obtained from turbine. In order to make the turbine operating at the maximum power point (MPP), a positive step change $\Delta\omega$ should be added to the reference speed command. With the increasing rotor speed, the turbine produces a higher output power. The difference of the power change is calculated for each time step.

$$\Delta P(k) = P(k) - P\ (k-1)$$

Since a positive speed change leads to a positive power change, this increase in power implies that the MPP is further on the right hand side of the current operation point. Thus a further positive variation of the reference rotor speed is required to make the output power moving to the MPP for this water speed. As the drawback of the hill-climb searching method, the optimal reference speed cannot be settled down at the MPP, and observation and perturbation method would keep the operation point vibrating around the MPP. Therefore, when ΔP is small enough (within a specific power range which is +/- 5% of normal generator power rating) no action would be taken on the reference speed and the system is regarded as working at the MPP. In addition, the size of step change $|\Delta\omega|$ is made proportional to the slope of ΔP. For a water speed with uniform acceleration speed, the slope of the power variation is constant, so the size of step change should be constant. Therefore, a large reference speed change is due to a large power change. When the operation point is close to the MPP, the step change would get smaller because the power change is getting smaller. This variable step change on the reference speed not only helps to locate the MPP accurately but also provides a significant improvement on the algorithm efficiency. The detailed selection of the step size is described next. After these dynamic changes on the rotor speed, the turbine is working on the MPP (P_1). Then a step jump happened on the water speed from v_1 to v_3. Since the turbine speed cannot change instantaneously (the inertia of the system is larger and the reference speed for the speed control is not changed yet), but the instantaneous power generated by the turbine is P_5 and a large positive power change is generated. Corresponding to this positive power variation, a large positive speed change is

required. Same detecting process as mentioned above will be used to find the MPP at this water speed. After that, assuming the water speed drops from v_3 down to v_2, so the output power changes from the MPP P_3 to P_6, which results a large negative change on the power. The operation point now is at the right hand side of the MPP curve. In order to pull the turbine operation point back to the MPP, the reference speed should be reduced, and thus a negative step change on the reference speed is commanded. Because the negative change is not enough to drag the operation point to the MPP, the operation point is still working at the right hand side of the MPP, and a further reduction on the reference speed is needed. But the output power is increased from P_6 to another power lower than P_2, a positive ΔP is obtained. Therefore, increasing or decreasing reference speed by judging the sign of ΔP may cause confusion on the algorithm. In order to solve this problem, a direction factor a is introduced into this algorithm. A table of relationship between the operation status and direction factors is listed below to illustrate the sigh of each parameter under different situations.

Table 3-1 Table of operation direction

Status	a	ΔP	$\Delta\omega$	a^*
Water speed increasing	$+$	$+$	$+$	$+$
Water speed decreasing	$+$	$-$	$-$	$-$
MPPT/Power regulation	$-$	$+$	$-$	$-$
Power regulation	$-$	$-$	$+$	$+$
a^*represents the updated direction factor that will be used for the next time step				

With the help of table 3-1, it can be seen that when the water speed is decreasing from v_3 to v_2, a reduction on the reference speed should be suggest due to the negative change on the power output. Because of the negative step change in reference speed, the direction factor has been turned to negative. For the next sampling period, even though there is a positive change on the output power, the reference speed should be continuously reduced until the operation point reaches to the MPP. What should be mentioned is that when the operation point approaches to the MPP, the direction factor will turn to positive. Based on this operation principle, the MPPT function can be realized when the water speed is between cut-in speed and rated water speed.

When the water speed increases from v_3 to v_4, the output power changes from P_3 to P_4, this is higher than the limitation of generator power rating. Therefore, the Power regulation is used, so that the output power does not exceed the power limit. When the output power is higher than the predetermined power limit ($P_7 = P_3$), a negative speed change will be applied to the reference speed to decrease the output power, and the TSR will be also reduced. Furthermore, the size of the step change on the reference speed depends on the power. Normally, when the water speed is higher than the rated water speed, the system operation status will switch between the MPPT mode and Power regulation mode.

The selection of the size of speed change is important in the algorithm. The magnitude of step variation is shown in [31]:

$$|\Delta\omega(k)| = |C_{step} * \frac{\Delta P\ (\mathrm{k})}{dt}|$$

C_{step} is the step change constant which determines the change in the speed reference depending on the variation of the power. The reference in [31] indicates that to choose the value of C_{step}, an approximate idea of turbine power characteristics is needed. As shown in figure 3-3, the slope of the optimal power point curve increases when the higher rotor speed presents, which means a higher water speed presents. Consequently, when the step change constant is set to be the maximum value of $\frac{\Delta\omega}{\frac{\Delta P\ (\mathrm{k})}{dt}}$ during high water speed condition, the increment of reference speed would be more than desired, and this increment could cause an overshooting of the optimal power point and the system would oscillate about the MPP before settling down. Additionally, a large value of step change constant can also result in a large transient in the generator torque that may damage the turbine system. Therefore, the value of step change constant C_{step} could not exceed the minimum value of $\frac{\Delta\omega}{\frac{\Delta P\ (\mathrm{k})}{dt}}$.

As mentioned above the power variation (ΔP) curve should be linear when the water changes linearly, which means the slope of the curve should be constant, however, fluctuations are always happened in the power curve. For example, figure 3-4 presents the case of the water speed increase from 1.5m/s to 3m/s linearly. It can be seen that the curve of the power change is increase linearly which means the slope of power change is constant. But there are fluctuation

occurred in the power curve and the oversize power change value might affect the step size selection and then influence the accuracy of MPPT algorithm. In order to reduce the effects of the fluctuations, the slope is calculated by averaging. For each time step, the new slope is added up to the sum of slopes (slope_total) and then the average value is calculated for the step change calculation. For different water speed situations, the slopes are different, and therefore, the sum value will be cleared to zero and a new slope value will be calculated for different operation directions like the table shown in Table 3-1. This slope calculation method is only used for the MPPT part, while the constant step sizes are used in the Power regulation mode.

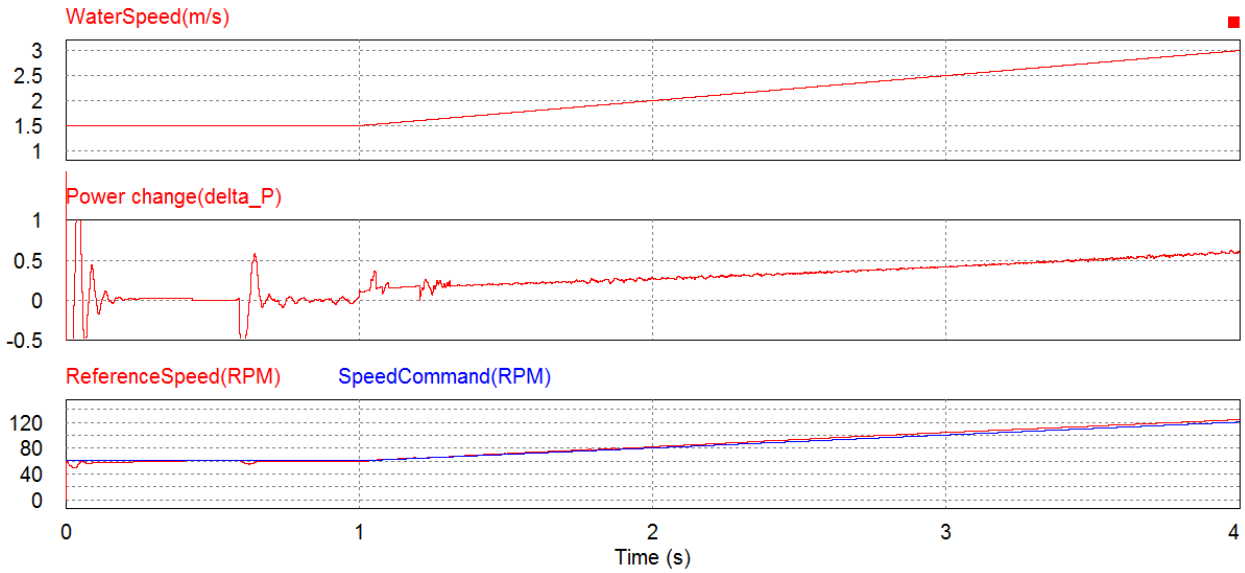

Figure 3-4 Example for slope calculation

Eventually, the choice of sampling frequency for the power conversion block is explained below. It is critical for the algorithm to work properly. The sampling period should be larger than the speed controller time constant. When the system is accelerating, the generator torque is instantaneously reduced, and as the driving torque increases, the system accelerates. Finally, as the rotor speed approaches the reference rotor speed, the generator torque equals to the turbine torque. If the generator power were computed during the period when the speed controller is active, it would mislead the system to the opposite direction. A sample taken immediately after the increment of the speed command would show that the generator power actually reduces. [31] The sampling period is assumed four times of rotor speed controller time constant.

The power conversion algorithms applied in this hydrokinetic system is described above. In some papers, an intelligent memory is added in the hill-climb searching method to store the

optimal points for later use if the water speed repeats. Certainly, this technique can improve the response time and gives an efficient speed command to achieve the optimal hydrokinetic power. Since the variation of water speed is not as frequent as wind speed, the memory storage is not necessary for the hydrokinetic system. Some of the memory mechanism requires the anemometer, because the optimal power point should be stored along with the corresponding water speed. In general, the hill-climb searching strategy is flexible for the sensor-less system without any information of turbine power characteristics while the digital coding method is easy to modify to adapt to different turbine configurations. The performance of hill-climb searching algorithm will be demonstrated in the simulation part in Chapter 4.

3.2 Control Strategies of PMSG

As discussed before, the PMSG is employed in this hydrokinetic system. In this section the control strategies of PMSG are discussed. Theoretically, the way in which the generator speed can be controlled is realized by adjusting the electrical loading on the system. From the equation 2.4, it is known that the water speed is uncontrollable, so the only way to alter the operating point is to control the rotor speed. Therefore, a variable speed generator control is required for the efficient hydrokinetic power conversion system, because the variable speed generator control which is generated from MPPT/Power regulation block enables the generator to rotate at the optimal speed, according to a particular water velocity to obtain the maximum available output power from the turbine.

3.2.1 Classification of control strategies

In the paper [30] the PMSG control is realized by adjusting the duty cycle of a DC/DC converter. As mentioned in Chapter 2, a diode bridge is connected directly between the generator and DC/DC converter. Because the rotor speed is proportional to the output voltage of generator and to the voltage on the DC bus, controlling the rotor speed by governing the duty cycle of the DC/DC converter is possible. This method has the advantages of easy implementation, but it is not possible for the power factor control and a high harmonic distortion will be introduced into the system.

The most popular way to realize the PM generator control is connecting the generator to a fully controlled frequency converter (active rectifier). In general, this control method can be divided

into scalar control and vector control. Figure 3-5 presents the general classification of the variable frequency control.

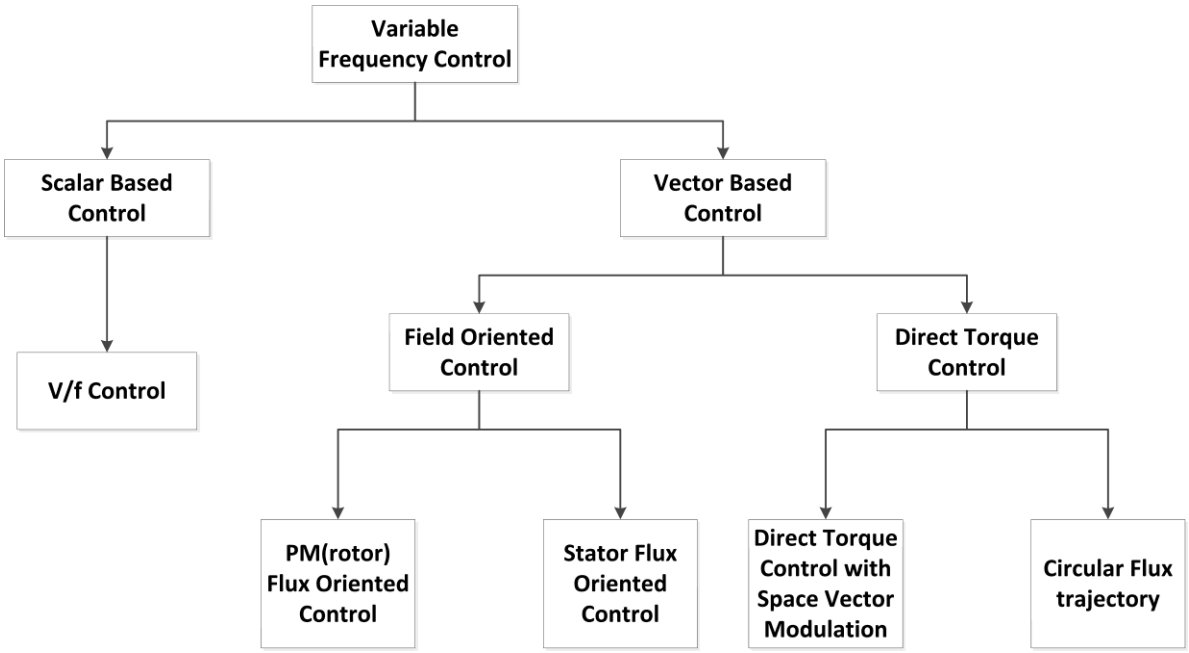

Figure 3-5 Classification of variable frequency control [18]

The scalar control methods are based on a valid relation in steady state, where only the magnitude and frequency of voltage, current and flux linkage space vector are controlled. The scalar control provides the simplest method to implement among the other control strategies, but it also gives an inferior performance. The open loop V/Hz control is the most popular scalar-control method with its simplicity and low-cost, and it is always used with induction machines or synchronous machines because their stator structures are identical. In this strategy, feedback signals are not required. For adjustable speed application, by neglecting the stator resistance, voltage is required to be proportional to the frequency or speed ($\omega = 2\pi f$) so that the stator flux ($\varphi_s = \frac{V_s}{f}$) keeps constant. [20] However the simplicity of the open loop V/Hz control and its ability to operate over a wide speed range, this scalar control method also has some drawbacks. For example, the performance of open-loop methods often depends on the motor parameters and the load conditions of the system, and such methods can experience power swings which might cause the machine to lose synchronism within specific speed ranges. In addition, V/Hz control method is not suitable for the low speed control in high dynamic application. [22]

Vector control provides superior performance and it has many advantages over scalar control. The vector control is valid for dynamic states, so not only the magnitude and frequency, but also the position of the voltage, current and flux space vector are controlled. In other words, the magnitude and angle of vector spaces are controlled. There are two vector-control methods, direct torque control (DTC) and field oriented control (FOC) which are the most commonly used in the machine control system.

The Direct Torque Control [23] was developed in the mid-1980s and introduced in the market by ABB. It has lots of advantages like good dynamic behavior and simpler control scheme without reference transformation frame and measurements for position and speed, thus being considered as sensorless control technique. The DTC scheme consists of torque and stator flux estimators, torque and flux hysteresis comparators, a switching table and a voltage source inverter. The key point of the DTC is to select an optimum voltage vector to control the electromagnetic torque and the stator flux simultaneously.

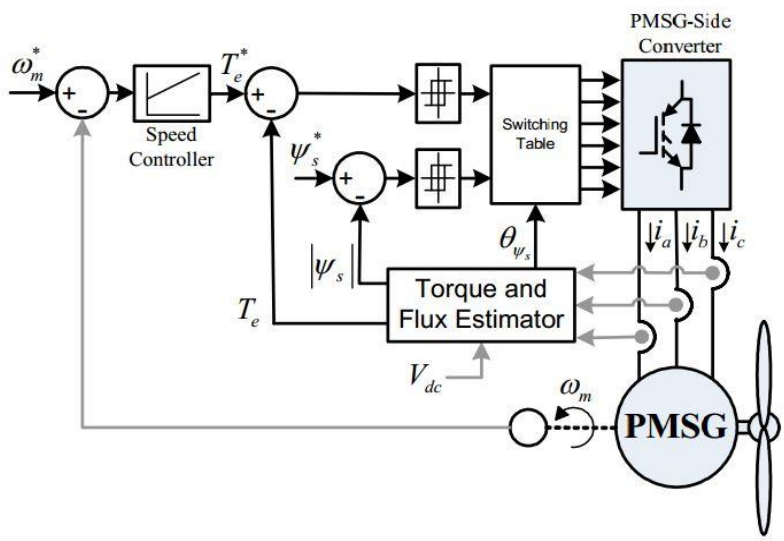

Figure 3-6 Schematic diagram of direct torque control [24]

As it is shown in figure 3-6, the stator currents and DC-link voltage are sampled and calculated in the flux and torque estimator. The estimated torque and flux magnitudes are compared with the reference values through the hysteresis comparator and then to the switching table which is used to select the corresponding voltage vectors for each time period. The drawback of the DTC is that a high switching frequency is required to avoid high torque and current ripple at the steady

state operation, and because the high switching frequency will generate excessive amount of heat, the cost for the electronic components in the drive system will increase.

The Field Oriented Control (FOC) is developed in the early 1970s, and because of its high performance, it becomes the most popular and widely used vector control strategy for controlling the torque and speed of Permanent Magnet Synchronous Machines. The general block diagram of FOC is presented in figure 3-7.

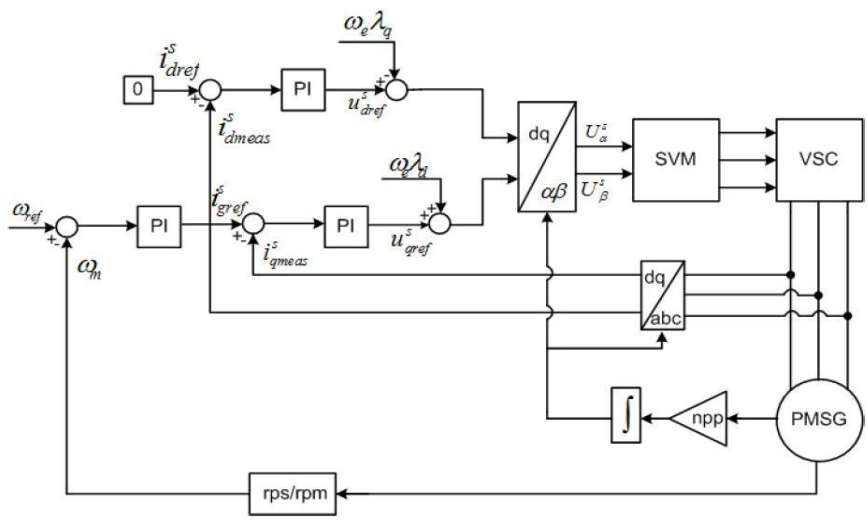

Figure 3-7 Schematic diagram of field oriented control [19]

FOC strategy is composed of two current controllers and one outer loop speed controller. They are all realized by PI control strategy due to its good steady state errors. The speed controller is in the outer loop which is a closed loop with the instantaneous shaft speed obtained from the speed sensor. The speed error is obtained by comparing the reference speed and the feedback value. The reference q-axis current can be generated from the outer loop speed controller and the reference q-axis current will also be used in the inner loop current controller. However, an important requirement is that the current controller must react faster on the input variations than the speed controller.

The objective of FOC strategy is to control the PMSM as a separately excited DC machine, such that the flux and torque can be controlled separately (in a decoupled way) [23]. In order to achieve separate control on flux and torque, the current controller operates in the d-q coordinate frame. The instantaneous three-phase stator currents are transformed into d-q reference frame,

and the transformation also requires the position of the rotor which is the integration of the shaft speed from the speed sensor. According to the equations of PMSG (2.15) & (2.18), the flux is controlled through the d-axis current while the torque is controlled through the q-axis current. Therefore, when a synchronous generator operates in a manner that the d-axis current is zero, the generator operates at the peak efficiency. In this case the amount of current flowing through the stator for a given amount of torque is smallest. Because more stator current leads to more heat generation and losses, minimizing stator current is required plus any current on the d-axis contributes to reactive power and does not contribute to the net conversion between mechanical and electrical power. [26] Consequently, the reference d-axis current should be set as zero. The control procedure is described in figure 3-7. The reference currents are compared with the sampled actual rotor currents in the d-q reference frame and sent to two current controllers. Because there is no neutral connection, the zero-sequence component is ignored and assumed to be zero. The difference between the desired stator currents (i_{dref}, i_{qref}) and the measured currents (i_d, i_q) are fed into the current controllers (PIs), and then the current controllers produce the voltage command signals (u_d, u_q). In figure 3-6, the d-q frame voltages are transformed to the $\alpha\beta$ reference frame by Park Transformation. The $\alpha\beta$ reference frame voltages are suitable for driving the Space Vector Modulation (SVM) method used to obtain the Pulse Width Modulation (PWM) signals for the active rectifier. In the simulation model, the d-q frame command voltages are transformed into the 3-phase Voltage (abc) directly by means of dq0/abc transformation block. The 3-phase voltage are scaled and compared with the carrier waveform to generate the PWM signals. The detailed method will be described in the simulation section. Moreover, term $\omega_e\lambda_d$and term $\omega_e\lambda_q$ are added to the controller output to linearize and decouple the two axes. The d-axis decoupling component is the product of electrical speed ω_e multiplied by d-axis magnetic flux λ_d, which result from the rotor permanent magnet flux λ_m and the magnetic flux generated in the stator coils:

$$d - axis = \omega_e\lambda_d = P_p\omega_g * (\lambda_m + L_d i_d) \tag{1.5}$$

For the q-axis decoupling components are similar but the contribution of the rotor permanent magnet is zero:

$$q - axis = \omega_e\lambda_q = P_p\omega_g * L_q i_q \tag{1.6}$$

These two decoupling factors are coming from stator voltage equations. Compensation terms are added to improve the dynamic response. By subtracting $\omega_e\lambda_q$ and adding $\omega_e\lambda_d$, the d-q currents will be independently of each other. Since the d and q current controllers have the same dynamics except for the decoupling components, the design of the PI controller can be same.

3.2.2 Detailed design of d and q axis current controller

The structure of d and q current controller is presented below in figure 3-8. The detailed explanations of each block are given:

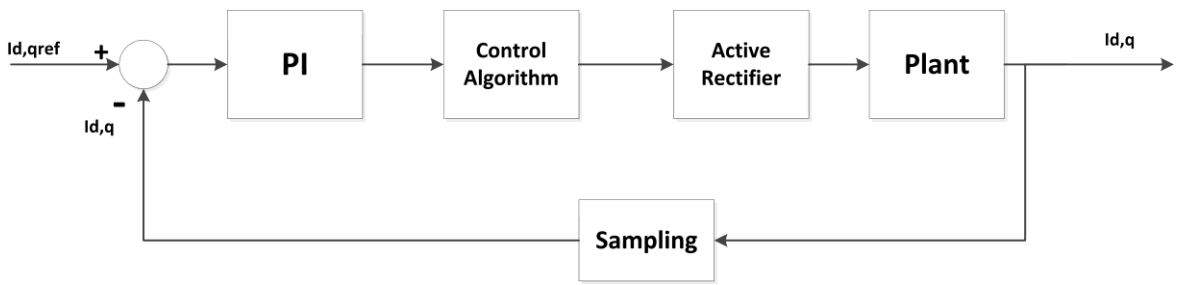

Figure 3-8 Control structure of d-q current control

Note that the decoupling components are small so they can be neglected from the diagram of the current controller, and the d-axis inductance and the q-axis inductance($L_d = L_q = 10.9mH, L_s = 6.3mH$) are equal to the stator inductance of the real generator which will be used in the bench testing. Therefore, the designs of d-axis and q-axis current controller are identical. The tuning of q-axis current PI controller is derived below. All the transfer functions are derived in the S - domain and the design idea is based on the A. Cimpoeru's paper [19]. All the parameters used in this design are from the selected real system components of bench testing, and the data sheets are shown in the appendix.

The PI controller block has the transfer function which is the ratio between the output signal and the error signal as shown:

$$G_{PI}(s) = k_{pi} + \frac{k_{ii}}{s} \tag{3.1}$$

Where $k_p$is the proportional gain, $k_i$is the integrator gain. The integrator time constant T_{ii} represents the ratio between k_{pi} and k_{ii}.

$$T_{ii} = \frac{k_{pi}}{k_{ii}} \tag{3.2}$$

So

$$G_{PI}(s) = k_{pi}\frac{1 + T_{ii}S}{T_{ii}S} \tag{3.3}$$

The transfer function of the control algorithm block is equal to the delay introduced from the digital calculation, and has the form of the first order transfer function with the time constant $T_s = \frac{1}{f_s} = 0.278ms$, where $f_s = 3600Hz$ is the sampling frequency.

$$G_{ca}(s) = \frac{1}{T_sS + 1} \tag{3.4}$$

The active rectifier can also introduce another delay which is equal to the voltage source inverter delay having the form of the first order transfer function, which is:

$$G_{ar}(s) = \frac{1}{T_sS + 1} \tag{3.5}$$

The plant transfer function is determined from the q-axis equivalent circuit without the decoupling term. The plant transfer function is simplified to a first order linear system:

$$G_{pl}(s) = \frac{i_q(s)}{u_q(s)} = \frac{1}{SL_q + R_s} = \frac{1/R_s}{S\frac{L_q}{R_s} + 1} \tag{3.6}$$

where L_q is the q-axis inductance and $R_s = 0.53\Omega$ is the stator resistance from Generator parameter Appendix A.

In order to simplify the function, $K = \frac{1}{R_s} = \frac{1}{0.53}$ is set as the inverse of the stator resistance and $T_g = \frac{L_q}{R_s} = 0.0205s$ is set as the generator time constant. So

$$G_{pl}(s) = \frac{K}{ST_g + 1} \tag{3.7}$$

The sampling block includes a delay introduced by sampling as half of sampling time. This block has a first order transfer function with the time constant T_s:

$$G_{sample}(s) = \frac{1}{0.5ST_s + 1} \tag{3.8}$$

After that, the open loop transfer function of current controller can be written as

$$G_{ol}(s) = G_{PI}(s) * G_{ac}(s) * G_{pl}(s) * G_{sample}(s) \tag{3.9}$$

$$G_{ol}(s) = k_{pi}\frac{1 + T_{ii}S}{T_{ii}S} * \frac{1}{T_sS + 1} * \frac{K}{ST_g + 1} * \frac{1}{0.5ST_s + 1} \tag{3.10}$$

Andreea Cimpoera's thesis work [19] described the detailed tuning method of the PI controller design. In order to make the system more stable, the slowest pole in the system has to be canceled out. This implies:

$$1 + T_{ii}S = ST_g + 1 \tag{3.11}$$

$$T_{ii} = T_g = 0.0205s \tag{3.12}$$

In order to simplify the transfer function, a time constant is introduced. Compared with the generator time constant, the values of delays introduced by the first order transfer function are very small. This implies that the transfer functions of the delay can be replaced by a unique transfer function of first order such that the time constant equals to the sum of all time constants from the system:

$$T_t = T_s + T_s + 0.5T_s = 2.5T_s \tag{3.13}$$

Then the open loop transfer function can be written as:

$$G_{ol}(s) = k_{pi}\frac{K}{T_{ii}S} * \frac{1}{T_tS + 1} \tag{3.14}$$

A controller design criterion called Optimal Modulus (OM) [26] with the damping factor as $\zeta = \frac{\sqrt{2}}{2}$ is used to determine the value of k_{pi}.

$$G_{om}(s) = \frac{1}{2\tau s(\tau s + 1)} \tag{3.15}$$

Therefore, to build the relationship between these two equations and calculate the gain of the PI controller:

$$k_{pi} * \frac{K}{T_{ii}S} * \frac{1}{T_tS + 1} = \frac{1}{2\tau s(\tau s + 1)} \tag{3.16}$$

$$k_{pi} = \frac{T_{ii}}{5KT_s} = 1.2 \tag{3.17}$$

So the PI transfer function in S-domain becomes:

$$G_{PI}(s) = 1.2 + \frac{58.53}{S} \tag{3.18}$$

Since the real system is a discrete system, the transfer function of the PI current controller should be transferred into Z-domain, as shown:

$$G_{PI}(Z) = 1.2 + \frac{58.53 * T_S}{Z - 1} = 1.2 + \frac{0.029}{Z - 1} \tag{3.19}$$

The Bode Diagram of q-axis open loop current control is presented in figure 3-9 below.

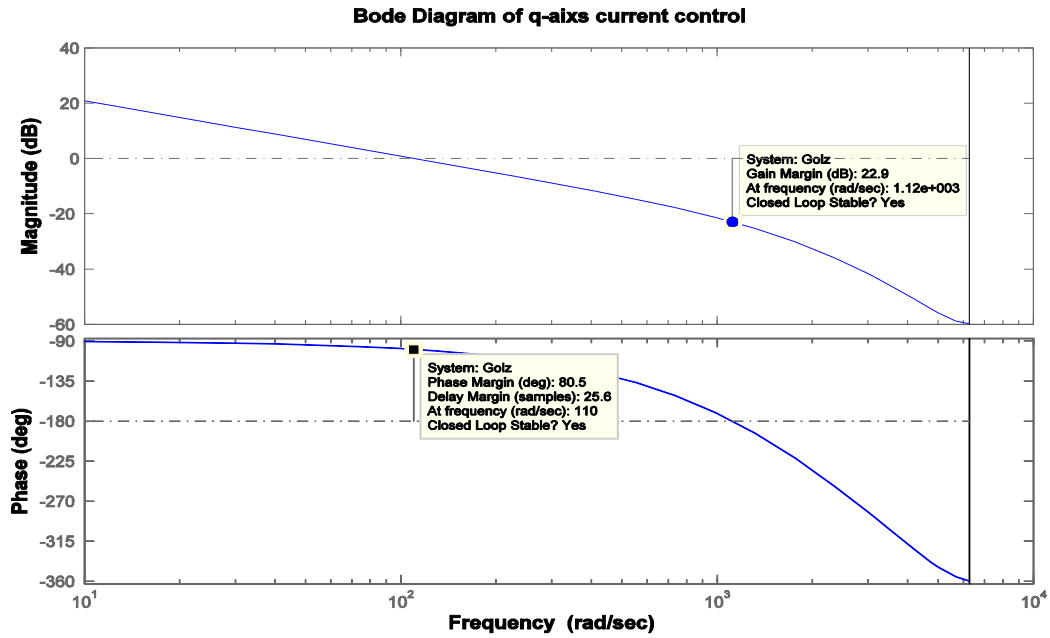

Figure 3-9 Bode diagram of the d-q current controller

It can be seen that it has the gain margin is 22.9 dB and the phase margin is 80.5 deg. The gain margin is greater than 7 dB and the phase margin is greater than 45 deg, so it indicates that the system is stable.

The step response of the d-axis current controller is shown in figure 3-9.

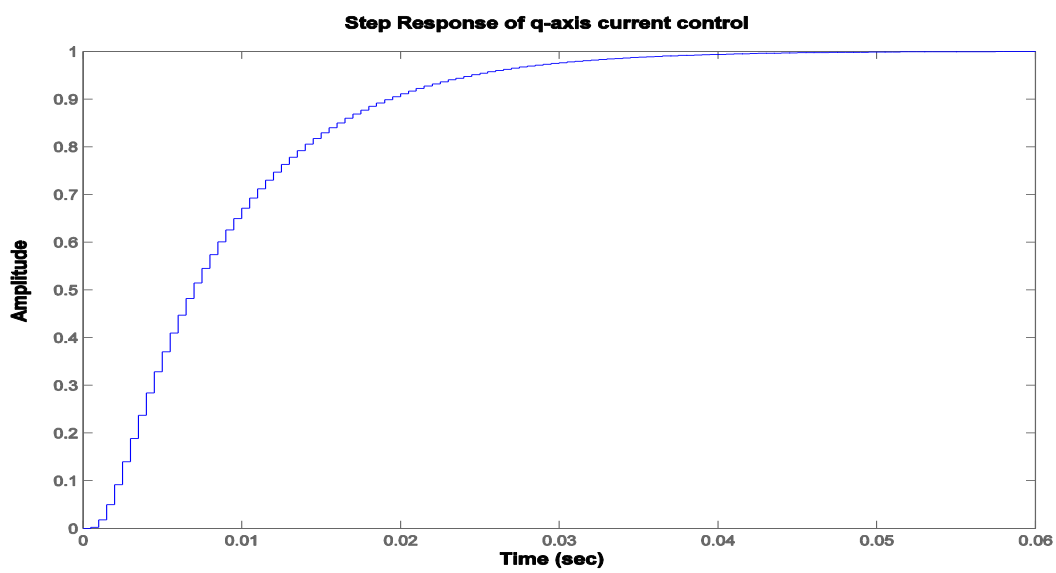

Figure 3-10 Step response of the d-q current controller

From figure 3-10, the response time is 0.05s, which means the controller is robust and fast.

3.2.3 Detailed design of outer loop speed controller [19]

The outer loop speed is used to calculate the reference value of q-axis current from the input of reference speed. The controller structure is shown in figure 3-11. In the controller loop, there are also different kinds of delays introduced in order to make the system realistic.

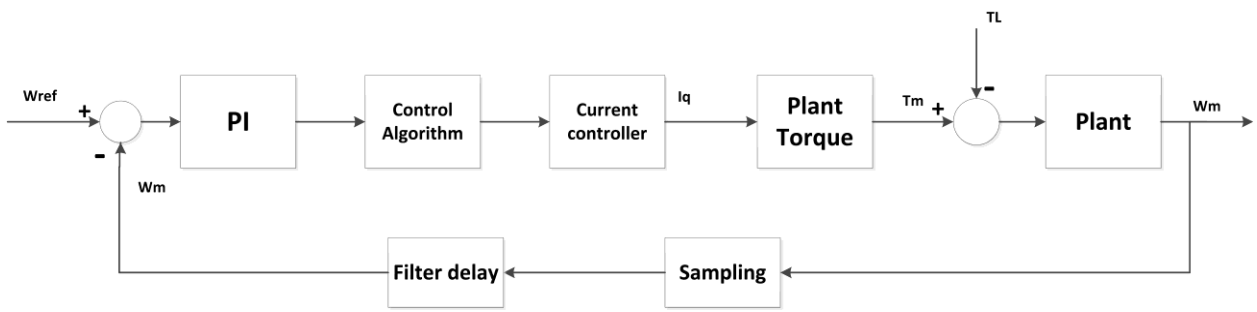

Figure 3-11 Control procedure of outer speed controller

The blocks in the loop are described in the following:

The PI speed controller block is the ratio of q-axis current signal and shaft speed error signal:

$$G_{PIs}(s) = k_{ps}\frac{1 + T_{is}S}{T_{is}S} \tag{3.20}$$

$$T_{is} = \frac{k_{ps}}{k_{is}} \tag{3.21}$$

Where $k_{ps}$is the proportional gain, $k_{is}$is the integrator gain. The integrator time constant of speed controller T_{is} represents the ratio between k_{ps} and k_{is}.

The control algorithm block, which is same as the one in the current controller, includes the delay introduced from the digital calculation. It has the form of the first order transfer function with the time constant $T_s = \frac{1}{f_s} = 0.5ms$, where f_s is sampling frequency same as above.

$$G_{ca}(s) = \frac{1}{T_sS + 1} \tag{3.22}$$

The current controller block includes a delay introduced by the current controller. It can be expressed as a first order transfer function:

$$G_{cc}(s) = \frac{1}{T_{iq}S + 1} \tag{3.23}$$

$$T_{iq} = \frac{T_{ii} * R_s}{K_{pi}} = \frac{0.0205 * 0.53}{1.2} = 9.05ms \tag{3.24}$$

where T_{iq} is the time constant of the current controller.

The plant block is the mechanical plant transfer function calculated from the PMSG equations (2.18 &2.19).

$$T_e - T_L - B = J\frac{d\omega_m}{dt} \tag{3.25}$$

$$T_e = \frac{3}{2}n_{pp}\Psi_m i_q^s \tag{3.26}$$

Where T_e represents the electrical torque, T_L represents the load torque, B represents the PMSG friction coefficient, J represents the inertia of the PMSG, n_{pp} represents the number of pole pairs, and $\Psi_m$represents the PMSG magnet linkage.

Since the friction coefficient is neglected, the mechanical equation can be written as:

$$T_e - T_L = J\frac{d\omega_m}{dt} \tag{3.27}$$

The load torque will not be considered from the view of the controller. So the plant transfer function described in S-domain is:

$$G_{pl}(S) = \frac{n_{pp}}{JS} \tag{3.28}$$

The sampling block includes a delay introduced by sampling as half of the sampling time. It is also a first order transfer function with the time constant T_s:

$$G_{sample}(s) = \frac{1}{0.5ST_s + 1} \tag{3.29}$$

The filter block includes a delay introduced by the filtering of speed measurement due to the encoder mounted on the machine shaft.

$$G_f(s) = \frac{1}{T_f S + 1} \tag{3.30}$$

$$T_f = \frac{1}{\omega_f} = \frac{1}{2\pi f_f} = 0.796ms \tag{3.31}$$

Where T_f is the filter time constant and $f_f = 200Hz$ is the cut off frequency of the speed sensor. Therefore, the open loop transfer function is presented in the equation:

$$G_{ops}(S) = G_{PIs}(s) * G_{ac}(s) * G_{cc}(s) * \frac{3}{2}n_{pp}\Psi_m * G_{pl}(S) * G_{sample}(s) * G_f(s) \tag{3.32}$$

$$G_{ops}(S) = k_{ps}\frac{1+T_{is}S}{T_{is}S} * \frac{1}{T_sS+1} * \frac{1}{T_{iq}S+1} * \frac{3}{2}n_{pp}\Psi_m * \frac{n_{pp}}{JS} * \frac{1}{0.5ST_s+1} * \frac{1}{T_fS+1} \tag{3.33}$$

In order to simplify the transfer function (3.33), all the delays can be combined into one approximate time constant T_{ss}:

$$T_{ss} = T_s + T_s + 0.5T_s + T_{iq} + T_f = 11.2ms \tag{3.34}$$

Then the transfer function (3.33) can be performed:

$$G_{ops}(S) = k_{ps}\frac{1+T_{is}S}{T_{is}S} * \frac{1}{T_{ss}S+1} * K_t * \frac{n_{pp}}{JS} \tag{3.35}$$

Where K_t=$\frac{3}{2}n_{pp}\Psi_m$.

From M. Roman's symmetric optimum method [26], a transfer function of this opened regulatory circuit is given to obtain an optimum response.

$$G_{op}^{som} = \frac{K_1K_pT_iS + K_1K_p}{s^2(T_1T_iS + T_1)} \tag{3.36}$$

In order to get the proportional gain of the controller, the open loop transfer function should be arranged in the same manner as a symmetric optimum equation.

$$G_{ops}(S) = \frac{\frac{n_{pp}}{J}K_tk_{ps}T_{is}S + \frac{n_{pp}}{J}K_tk_{ps}}{S^2(T_{is}T_{ss}S + T_{is})} \tag{3.37}$$

The adjustable PI controller gain can be deducted out with these equations:

$$K_{ps} = \frac{1}{2K_1T_1} = \frac{1}{2\frac{n_{pp}K_t}{j}T_{ss}} = 0.1 \tag{3.38}$$

$$T_{is} = 4 * T_1 = 4 * T_{ss} = 0.044s \tag{3.39}$$

Therefore, the speed controller transfer function in S-domain is:

$$G_{PI}(s) = 0.1 + \frac{2.27}{S} \tag{3.40}$$

For the real discrete system implementation the transfer function should be transferred into the Z domain:

$$G_{PI}(Z) = 0.1 + \frac{2.27 * T_S}{Z-1} = 0.1 + \frac{0.001136}{Z-1} \tag{3.41}$$

Figure 3-12, which is a Bode diagram shows that the gain margin and phase margin respectively are GM=33.4 dB and PM=50.5 deg. Therefore, the system is stable.

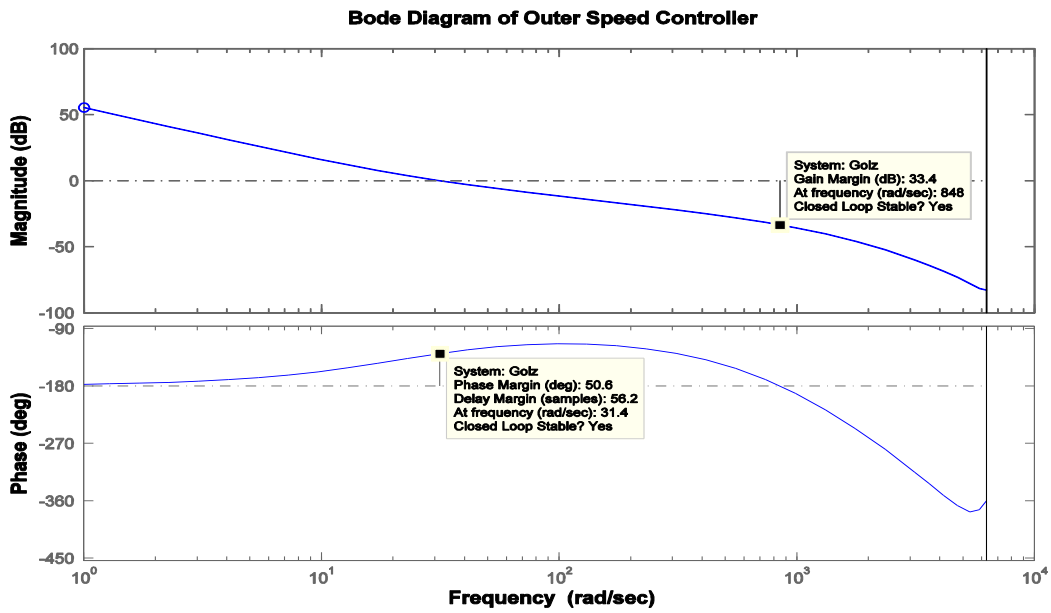

Figure 3-12 Bode diagram of the outer speed controller

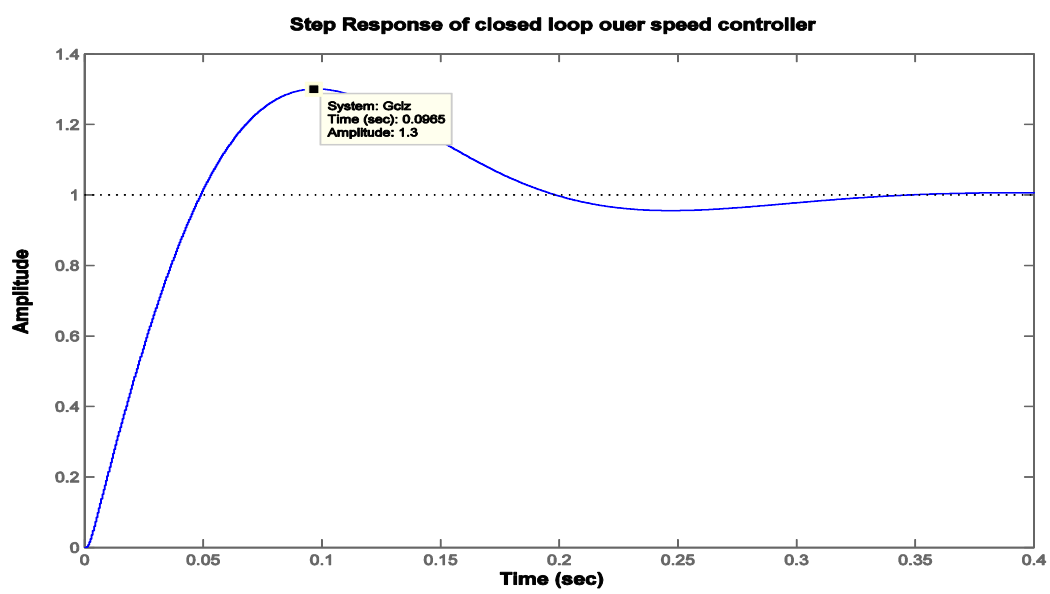

Figure 3-13 Step response of outer speed controller

Figure 3-13 shows that the maximum overshoot is 1.3 ($M_p = 30\%$) and the response time is 0.4s. Because the overshoot of the speed controller step response is very high, which means a very high torque may be applied when starting the machine. The large torque will cause the current to be enormous in amplitude that exceeds the maximum current limitation. Therefore, a limiter is required for this issue.

Chapter 4 – System Modeling and Simulation in PSIM

For the first part of this chapter, components of the final system configuration are simulated in the PSIM software based on the operation principle. The characteristics of each component are implemented and proved in the simulation model. In the end, all the components are integrated into the hydrokinetic power system. The most important function of this system simulation is to ensure the feasibility of the system design, and to indicate the excellent performance of the power conversion and control strategies if maximum power can be extracted from the water. In the second part, several cases under different water conditions are emulated with this proposed system model. The analysis and comparison of each case study result are provided. These case studies can not only demonstrate the validation of the system but also show the standard results for the hardware testing.

4.1 Hydrokinetic Turbine Model

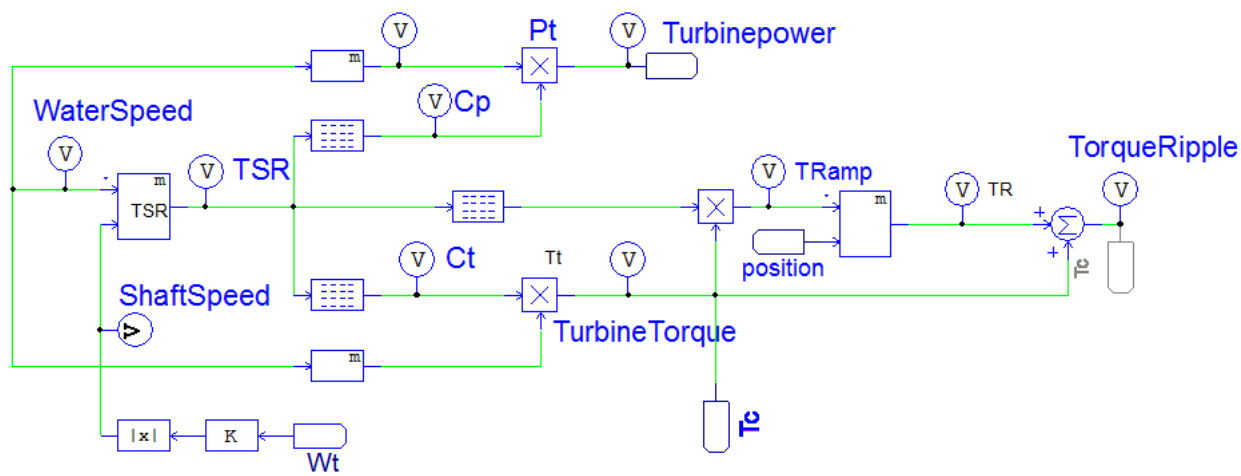

Figure 4-1 Simulation model of hydrokinetic turbine

The hydrokinetic turbine model is built based on the mathematical modeling of the hydrokinetic turbine. The objective of this hydrokinetic turbine model is to produce the output power and the torque for different water situation like the real turbine. As shown in Figure 4-1, the inputs to the turbine model are water speed V_w and the rotor speed ω_t measured from a rotational speed encoder. Then the instantaneous TSR value is calculated. The corresponding power coefficient and torque coefficient are selected by inputting the TSR into the lookup table blocks. The curves of the lookup table are shown in figure 4-2 and figure 4-3. In those figures, the x-axis represents

the TSR and the y-axis represents the power and torque coefficients respectively. The output power and torque of the turbine can be calculated based on the equation 2.3 & 2.6.

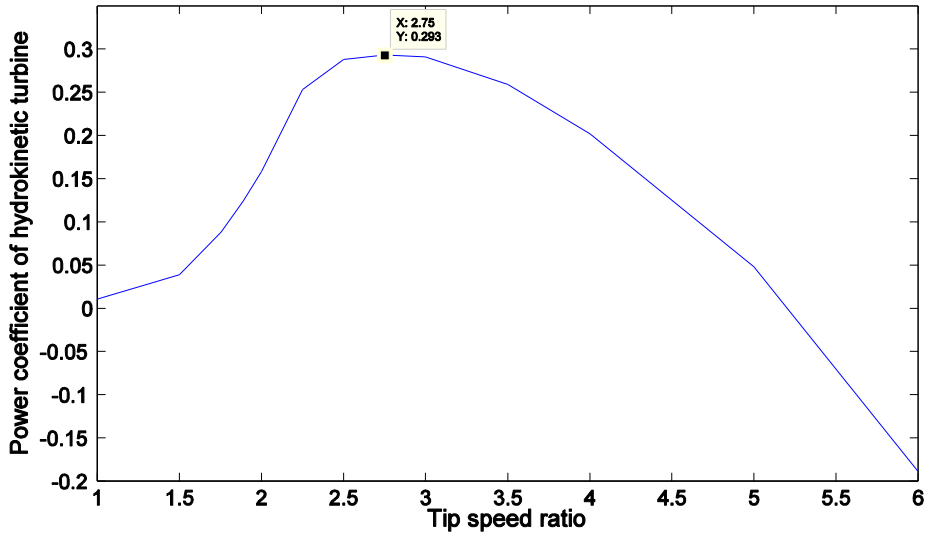

Figure 4-2 Curve of turbine power coefficient vs. TSR

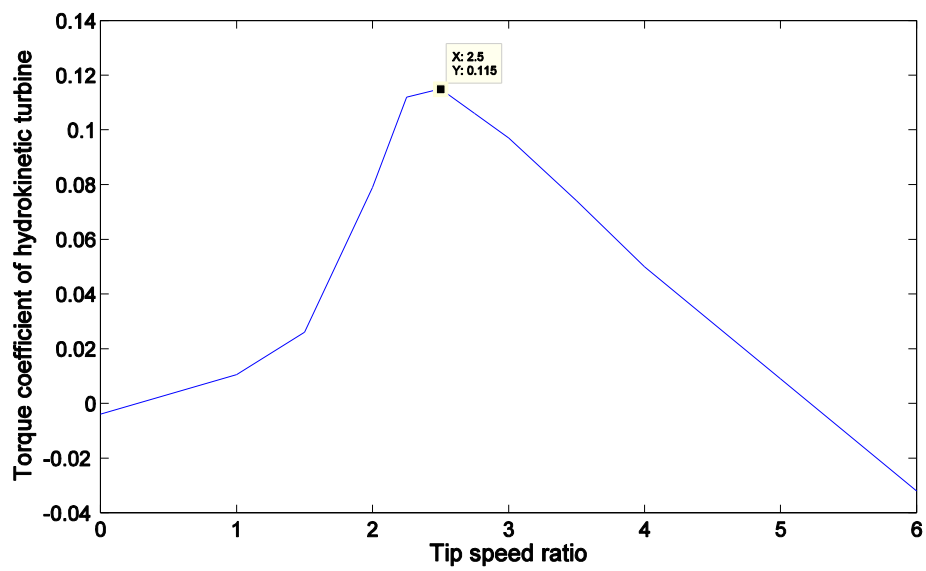

Figure 4-3 Curve of torque coefficient vs. TSR

Each turbine has its own coefficient curves which are provided by the turbine designer (Mavi Innovations Inc.). From the power coefficient curve, the maximum power coefficient is found ($C_p = 0.293$) when the TSR is 2.75. And for the torque coefficient curve, the optimal TSR is 2.5, which is different from power coefficient's optimal TSR. In addition, if the TSR value is higher

than 5, the power and torque coefficient will become negative, so the rotor speed should be controlled to maintain the TSR at the optimal value.

Another mechanical phenomenon should be mentioned is the torque ripple produced by the hydrokinetic turbine. The factors which contribute to the development of torque ripple include variation of water magnitude and direction, blade dynamics, blade stall and torsional slack in the drive train. If the torque ripple is sufficiently large, torque ripple will have a detrimental effect on the fatigue life of various drive train components (such as shafts, couplings and transmissions) and on the quality of output power. [33]

The torque ripple in the model is represented by a sinusoidal wave. The amplitude is the product of turbine torque T_t and torque ripple coefficient K_c, and the coefficient is from the lookup table (Figure 4-4). A position encoder on the shaft is used to determine the phase angle θ of the torque ripple. The shaft angle is multiplied by three to imitate each individual blade passing.

$$T_r = 0.5 * T_t * K_c * \sin(3 * \theta)$$

The turbine output torque is a combination of the torque ripple and calculated turbine output power.

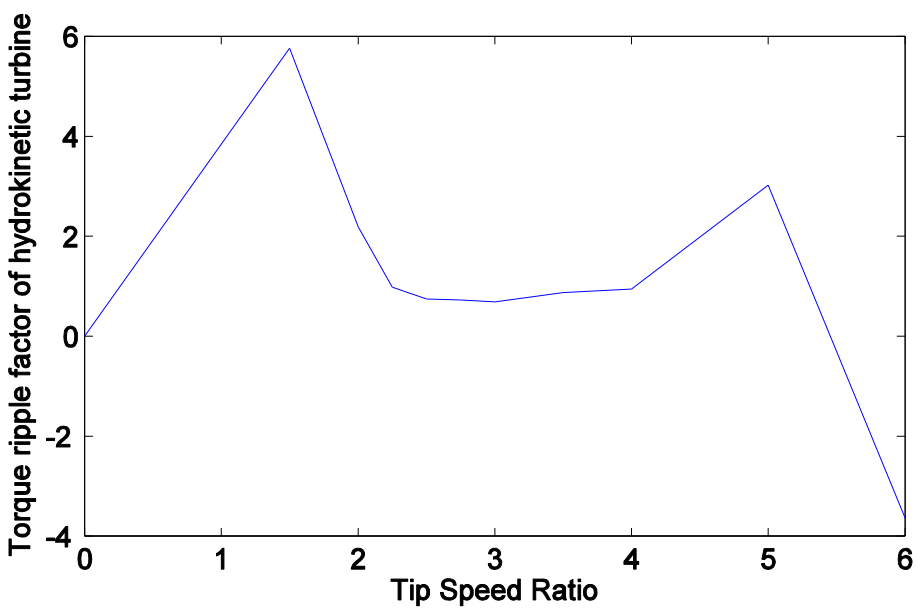

Figure 4-4 Curve of torque ripple coefficient vs. TSR

The torque ripple is the mechanical characteristic of turbine, and its values will be obtained from the turbine field-testing, so the effect of the torque ripple is not included in the case studies in Chapter 4. The main objective of this project is to demonstrate the power conversion and control system.

4.2 Mechanical/Electrical Interface Model

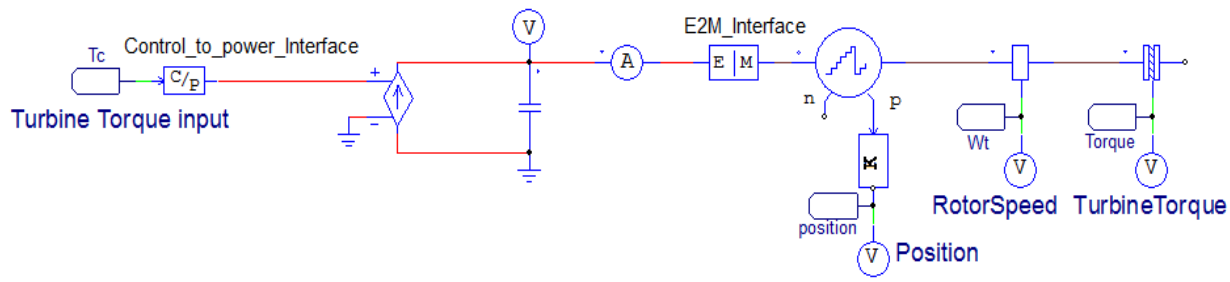

Figure 4-5 Simulation model of mechanical and electrical interface

In PSIM, there is a relationship between the electrical parameters (current, voltage, and capacitance) and the mechanical parameters (torque, angular rotational speed, and inertia), which are used to create a custom mechanical model. As shown in figure 4-5, the green line represents the control signal, the red line represents the power signal and the brown line represents the mechanical signal. In order to use the electrical quantity to represent the mechanical quantity, the mechanical and electrical interface block is used to realize the connection between the turbine model and generator model. The conversion rules between the mechanical and electrical in PSIM are shown below:

Voltage source represents Shaft Speed

Current source represents Torque

Capacitance represents Inertia

Capacitor initial voltage represents Turbine Initial Speed

Therefore, the torque produced by the turbine, which would drive the generator, is represented by the controlled current source. The capacitor is representing the total turbine inertia ($25.22 kg/m^2$), which includes the inertia of the turbine system, including the inertia of turbine blades, brake and shaft. A speed sensor and a torque sensor are used to measure the shaft speed and torque respectively. In order to calculate the torque ripple, an absolute encoder is employed to measure the position of the rotor.

4.3 Permanent Magnet Synchronous Generator Model

The PMSG model is selected from the PSIM simulation library. The characteristics for simulation can be obtained by setting the parameters to be the same as the real PMSG that will be used in the hydrokinetic system. The parameters of the PMSG are shown in appendix A. As discussed in Chapter 2, due to the advantage of multi-pole low speed PMSG, there is no need for a gearbox between the turbine and generator set, and hence, the generator model connects the turbine shaft directly. In the PMSG block, the mechanical power will be transformed into the 3-phase electrical power.

4.4 AC/DC PWM Active Rectifier Model

In the hydrokinetic system, the functions of the rectifier and rotor speed controller are realized by the Variable Frequency Drive (VFD). Generally, the PWM active rectifier comprises of six power electronic transistors – Insulated-Gate Bipolar Transistors (IGBTs). Therefore, the same configuration is simulated in the PSIM model. Six IGBTs are controlled by the PWM signals to convert the 3-phase AC power to the DC power.

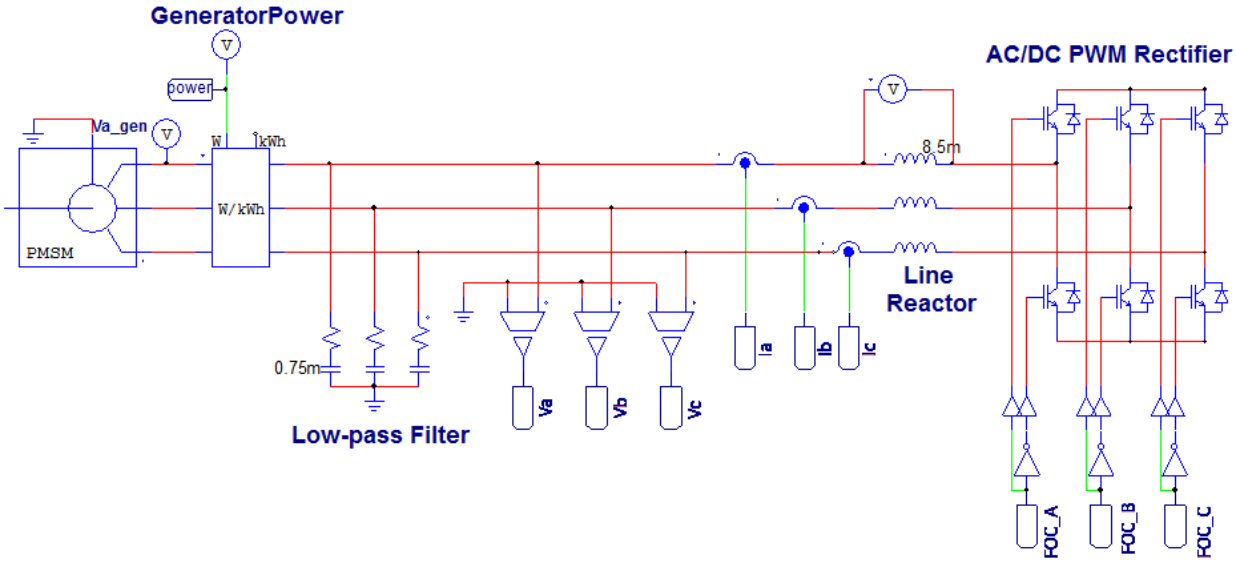

Figure 4-6 Simulation model of AC/DC PWM rectifier

Because the use of the power electronics transistors can introduce harmonic components to the generator output current, a filter and a line reactor are required in this rectifier. The parameters of these components are calculated in Chapter 2. As shown in figure 4-6, a series of measurement probes are applied in the model such as a 3-phase power meter, current and voltage meters.

4.5 Rotor Speed Controller Model and MPPT/Power regulation Block

4.5.1 Model of rotor speed controller

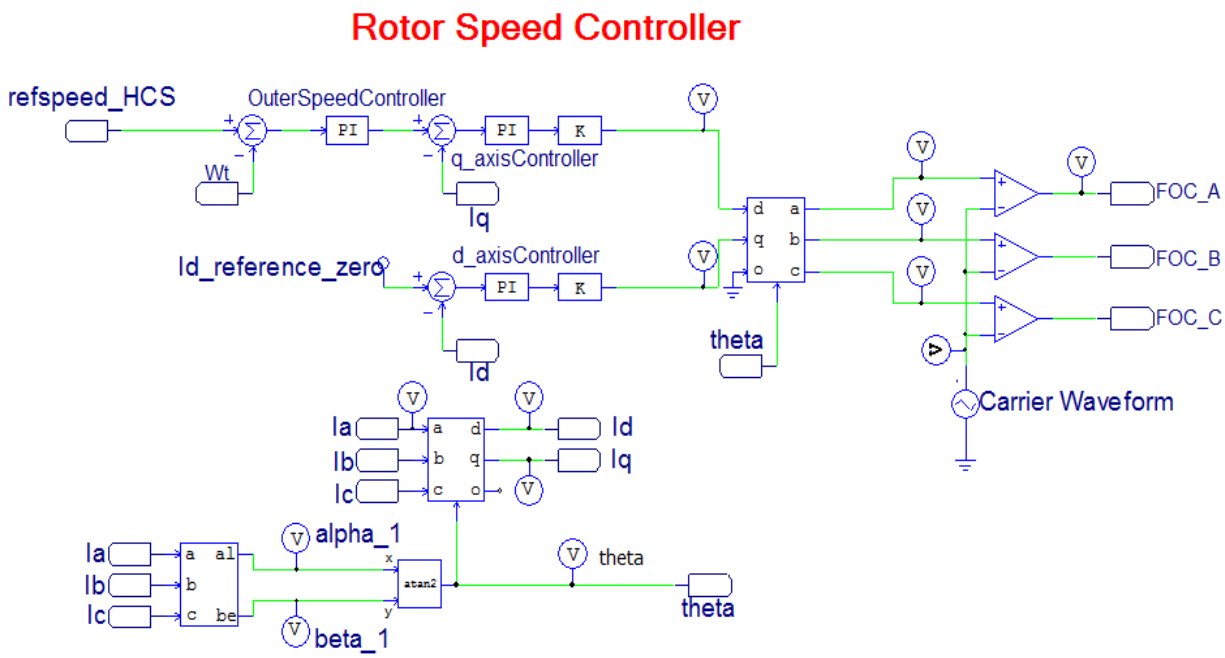

Figure 4-7 Simulation model of shaft speed controller

Figure 4-7 shows the PMSG rotor speed controller model. This rotor speed controller model is built based on the operation principle which has been described in Chapter 3. The input of the controller is the speed command ("refspeed_HCS") from the MPPT/Power regulation block and the output of the controller is the PWM signal which would be used as the gate switching signal for the IGBTs. In order to control the generator current in the d-q reference frame, the 3-phase currents have to be measured and transformed to the d-q coordinate frame by the abc/dq0 transformation block. Since the abc/dq0 transformation block requires the angle between the rotating and fixed coordinate system externally, the abc-to-alpha/beta transformation block is used to calculate the angle "theta". As shown in the controller model, the d-axis reference current is set as 0 in order to increase the efficiency of the system and reduce the reactive power components, and the q-axis current is obtained from speed command input through the outer loop speed controller. Then the d-q axis current controllers produce the corresponding d-axis voltage and q-axis voltage, which will be transformed to the 3-phase voltages by the dq0/abc transformation block. After the transformation, the 3-phase voltages will be compared with the

carrier waveform (3.6 kHz triangular wave) to produce the PWM signal. The demonstration of the controller is shown in section 4.7.

4.5.2 Selection of switching frequency and IGBT resistance

The efficiency of an AC/DC converter is one of the most significant attributes to consider when designing a power conversion system. Poor efficiency translates into higher power dissipation. Therefore, for the rectifier composed of IGBTs the switching frequency has a vital impact on the efficiency of the system. When using a high switching frequency, the motor noise and harmonic components can be minimized. Another advantage of using high switching frequency is the smaller values of capacitor and inductor. Increasing the switching frequency can reduce the capacity of the VFD and increase the components losses, like conduction losses and switching losses (turn-on losses and turn-off losses) and heat damage in the IGBTs. Additionally, higher switching frequency can produce more heat in the IGBTs. Thus, the cost of the components would be increased if adopting high-level IGBTs, like more advanced semiconductors, better quality reactive components, and more expensive thermal management. Furthermore, higher frequency can increase the losses caused by R, G, L and C of a long transmission line. Therefore, the best operating frequency is the lowest frequency compatible with the application's requirement for performance and cost.

But when the switching frequency increases, the harmonic components decrease as well as the harmonic losses. When harmonic losses are equal or higher than the IGBT losses (conduction losses and switching losses), the efficiency with higher switching frequency is equal or higher than the efficiency with lower switching frequency, but such observation does not set the switching frequency free from an upper limit. Even though higher switching frequency can reduce the harmonics and produce a smoother output power, thermal problem should be also concerned as the IGBTs can be burnt down by the heat. In order to select the optimized switching frequency, the cost-effectiveness problem should always be taken into account.

In the VFD manual, the range of switching frequency for the designate VFD is from 1 kHz-10 kHz (Default: 3.6kHz) [15]. In conclusion, the cost-efficiency of the components should be considered when selecting the system switching frequency. Based on the recommendation of the VFD manual and the efficiency tests above, the switching frequency is selected as 3.6 kHz.

In order to implement the characteristics of the real VFD, the IGBT transistor resistance is added to make the efficiency of the simulation model equals to the power efficiency of the VFD.

The VFD power losses with respect to switching frequency are shown as a function in the manual of the VFD. From the figure 4-8, if the switching frequency is 3.6 kHz, the power loss of the corresponding VFD is 1.2kW, and the efficiency of the VFD can be calculated by the function of:

$$\eta = \frac{P_{rated} - P_{loss}}{P_{rated}} = \frac{24kW - 1.2kW}{24kW} = 95\%$$

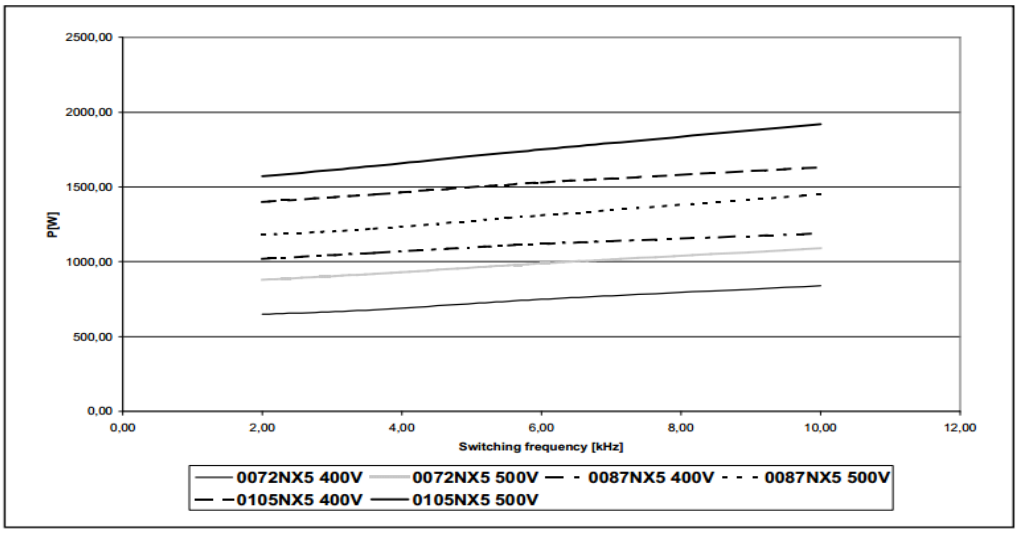

Figure 4-8 VFD power losses as function of switching frequency [15]

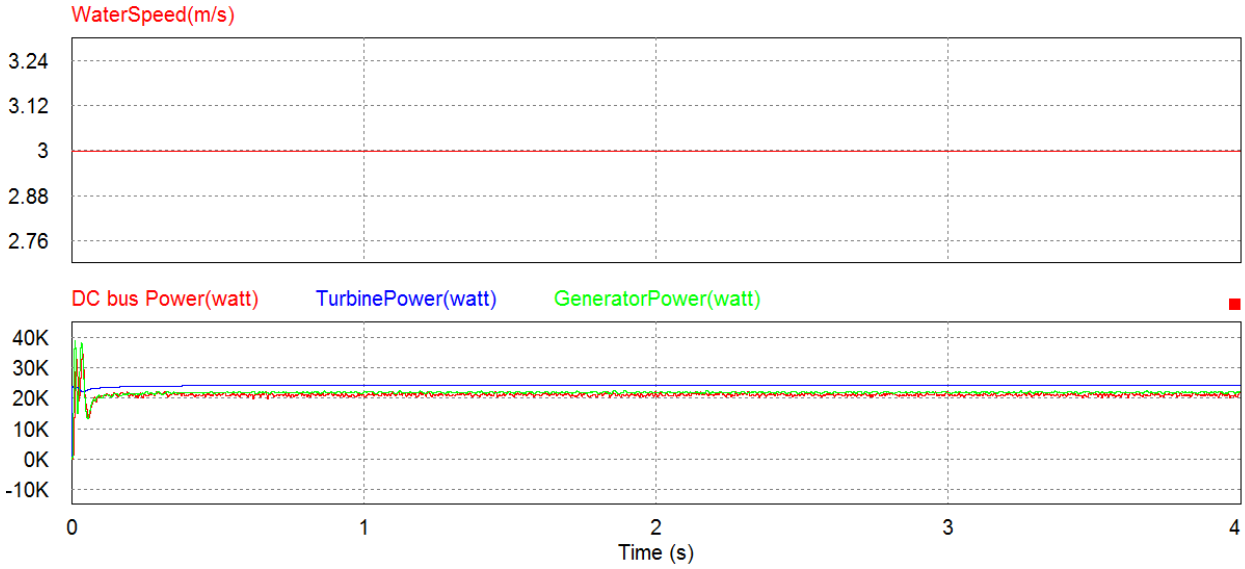

Figure 4-9 Hydrokinetic system simulation results with water speed at 3m/s

In order to realize the same efficiency as the real VFD, the transistor resistance is set as 0.2 ohm and the diode resistance is set as 0.05 ohm for each of IGBT switches. The water speed is assumed to be at the rated speed of 3m/s, so the simulation results are obtained in figure 4-9. As shown, the power on the DC bus is 21.15kW, the power output from the generator is 21.93kW and the turbine output power is 24.14 kW, so the efficiency of the IGBT switches is 95% which is same as the efficiency of the VFD. The efficiency of the generator for this water speed condition is 90.8% and the efficiency of the whole hydrokinetic system is 87%. At the very beginning of the figure, there is a very high transient happened, because the generator power and the DC bus power are starting at zero which the turbine power is initialized as 24kW. In order to increase these two powers to the steady state value in a short time, the transient happens.

4.5.3 MPPT/Power regulation block

In the MPPT/Power regulation block, there are two methods applied in this hydrokinetic system. One is the proposed hill-climb searching method (figure 4-10). In the model below, the C block is used as the MPPT/Power regulation block. The advantage of the C block is that the C code can be entered directly without compiling and hence, the hill-climb searching algorithm is written in the C code, which is shown in the appendix B. The input of the model is the power output from turbine (“Turbinepower”) and the output is the speed command (“refspeed_HCS”).

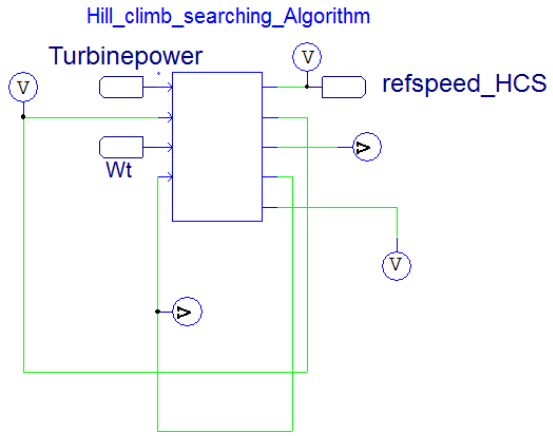

Figure 4-10 Simulation model of hill-climb searching algorithm

The other one is lookup table method (Figure 4-11) for which the relationship between the reference speed and instantaneous water speed is preprogrammed in a lookup table. The lookup table curve (Figure 4-12) is drawn by keeping the TSR at optimal value which is 2.75 for the MPPT operation status, and reducing the TSR maintains the output power at rated power for the

power regulation status. The input to the lookup table is the water speed (m/s) and the output of the table is the reference speed in rad/s, which is shown in the figure below.

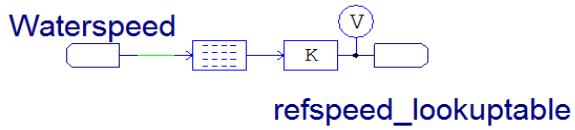

Figure 4-11 Simulation model of lookup table algorithm

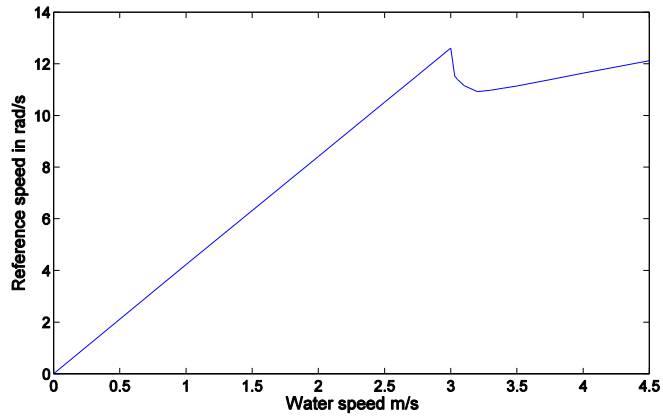

Figure 4-12 Lookup table curve of reference speed vs. water speed

The simulation results of these two methods would be used to demonstrate the characteristics of these different strategies.

4.6 DC Bus and DC Bus Chopper model

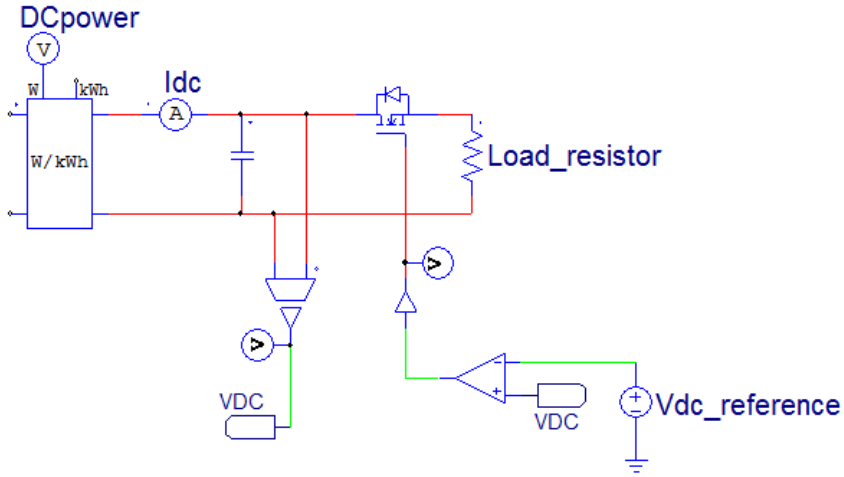

Figure 4-13 Simulation model of DC bus and DC bus chopper

The DC bus which is called as DC link is the main part of the VFD. The bus comes with a capacitor which is used to filter and smooth the DC voltage on the DC bus.

For the stand-alone system, a load resistor is attached on the DC bus to consume the excessive power produced by the hydrokinetic system. For this simulation system, a load resistor is used to dissipate all the power generated by the hydrokinetic system and a DC chopper switch is used to keep the DC voltage at a specific level, shown in figure 4-13. The DC bus chopper is controlled by a transistor switch, and when the DC bus voltage is higher than the reference DC bus voltage, the load resistor will be switched into the DC bus to consume the extra power until the DC bus voltage drops down to the reference voltage. Therefore, the voltage of DC bus can be maintained at a constant value for any load power.

4.7 Results of Cases Studies in PSIM

After the entire system is built up, several cases are simulated with this hydrokinetic model. Because the water speed is variable and unstable, to investigate and analyze the outputs of the hydrokinetic system for different water conditions is significant. In order to demonstrate the function of MPPT/Power regulation and the rotor speed controller, five cases are tested in this section.

4.7.1 Case 1—Water speed increases from 1.5m/s to 4.5m/s with lookup table method

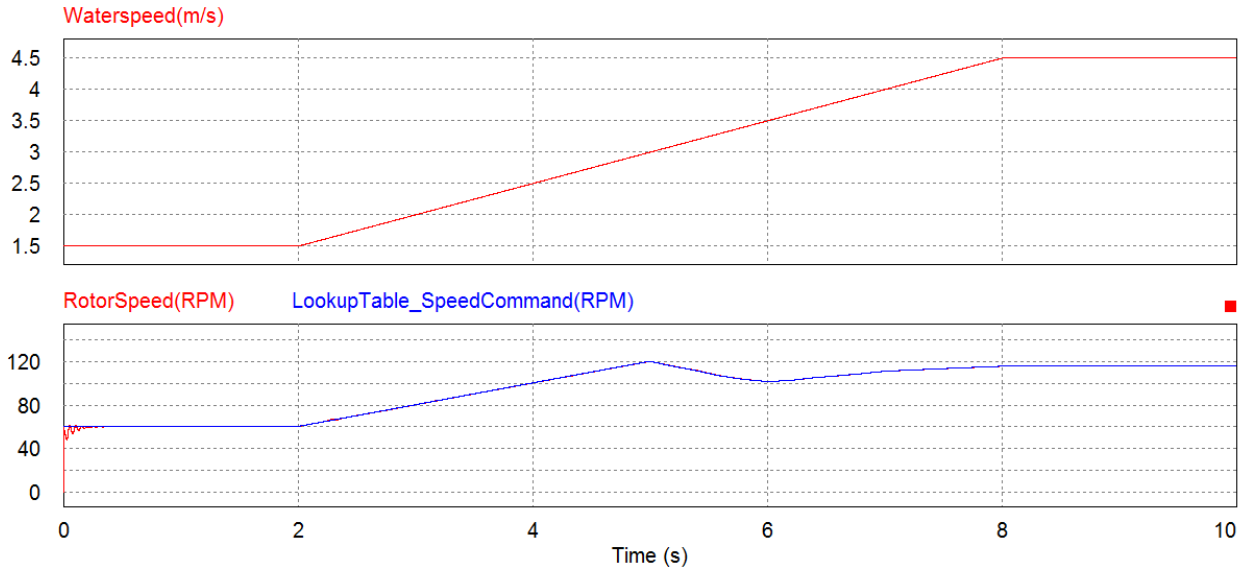

Figure 4-14 Water speed and speed commands of Case 1

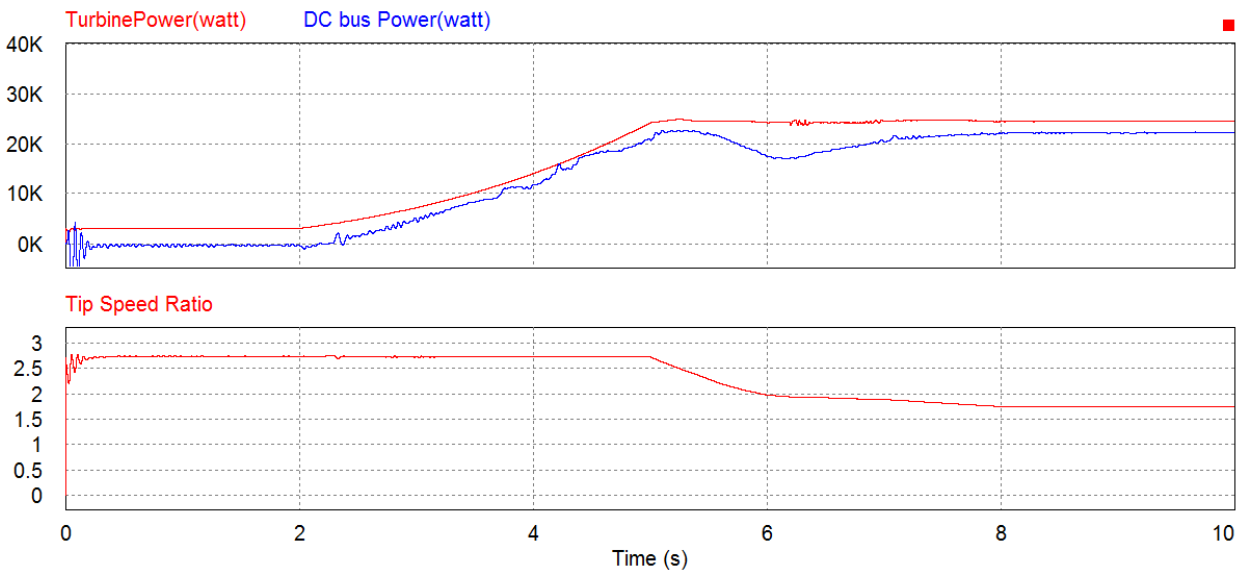

Figure 4-15 TSR and power outputs of Case 1

In this case, a variable water speed starts given from 1.5m/s, and raises to 4.5m/s for a period of 10s. The initial speed of the turbine is assumed as 60 RPM, which can avoid the initialization problem. In this case, the hydrokinetic system operates in the MPPT region for the first 5s and operates in the Power regulation region for the rest of the time. Because the curve of water speed versus optimal rotor speed has been already loaded into the lookup table, the speed command can be output to the rotor speed controller immediately. In figure 4-14, the actual rotor speed is identical to the speed command, which means the rotor speed controller is responding fast and robustly. In figure 4-15, when the MPPT function maintains the TSR of the turbine at the optimal value (2.75), the hydrokinetic system is operating at the maximum power point. When the water speed is higher than 3m/s, the power regulation keeps the turbine output power less than the power limitation (24.2kW) and the TSR is reduced. In general, the lookup table method is a straightforward strategy with the advantages of simple structure and efficient algorithm, but it always requires the water speed as the input to the lookup table. Furthermore, the results of the lookup table method are always used as reference options.

4.7.2 Case 2—Water speed increases from 1.5m/s to 4.5m/s with hill-climb searching method

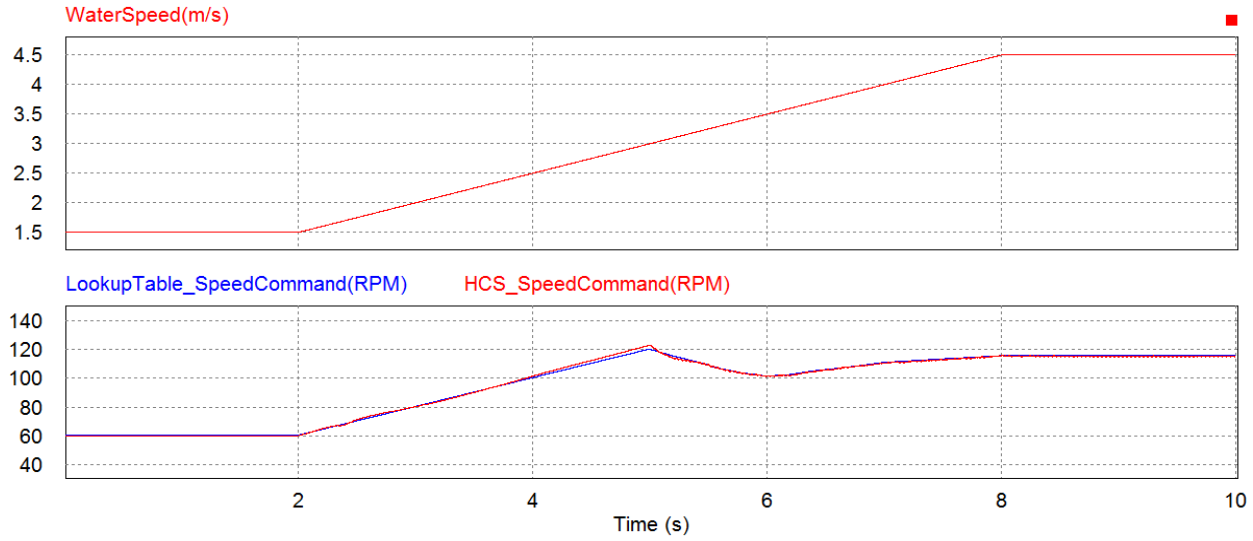

Figure 4-16 Water speed and speed commands of Case 2

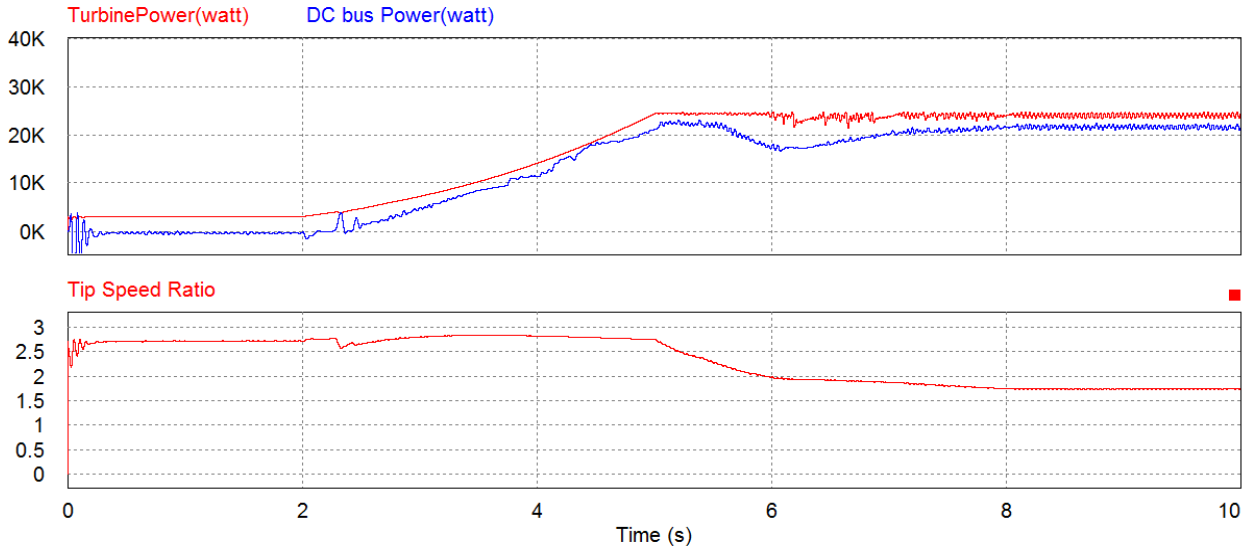

Figure 4-17 TSR and power outputs of Case 2

In this case, the water situation is same as Case 1, but the hill-climb searching method is used instead of the lookup table method. The initial speed is set as 60 RPM, but it still needs to start from zero at the very beginning. For this reason, a short time oscillation happens. With the rising water speed the hill-climb searching method tracks the turbine power change and the speed controller controls the rotor speed by the speed command output from the MPPT block. By comparing with the reference speed obtained from a lookup table in figure 4-16, the speed command obtained from hill-climb searching method is coincident. In the figure 4-17 when the

water speed is higher than 3m/s, the power regulation strategy maintains the turbine output power at the rated generator power (P_limit=24.2kW) by changing the rotor speed. Therefore, the TSR decreases from 2.75 to 1.75 and the rotor speed decreases from 120 RPM to 100RPM and raises back to 116RPM.The error between the DC power and the turbine power is caused by the system losses, like generator losses and IGBTs losses.

From both case 1 and case 2, it can be seen that the curves of turbine power are nearly identical with figure 3-1 (system operation status), which means the hydrokinetic system is operating at the MPP during the whole period. Therefore, the design of MPPT and Power regulation strategy is working as expected. Comparing with lookup table method, the hill-climb searching method might introduce more oscillations to the output power. Due to the observation and perturbation algorithm used in the hill-climb searching method, it cannot response as fast as the lookup table method, but this hill-climb searching method can be used with different types of machine without knowing any characteristic information of the machine. In addition, the errors produced by the hill-climb searching method are small and negligible for this hydrokinetic system.

4.7.3 Case 3—Constant water speed with a small ripple

In this case, a small ripple (magnitude change +/- 0.5) is added in the constant water speed (3m/s) to imitate the turbulence or eddies occurring in the river. The objective of this case is to demonstrate the feasibility of the rotor speed controller and MPPT/Power regulation function when fluctuation happened in the constant water speed. The results of lookup table method are used as the target results for comparing.

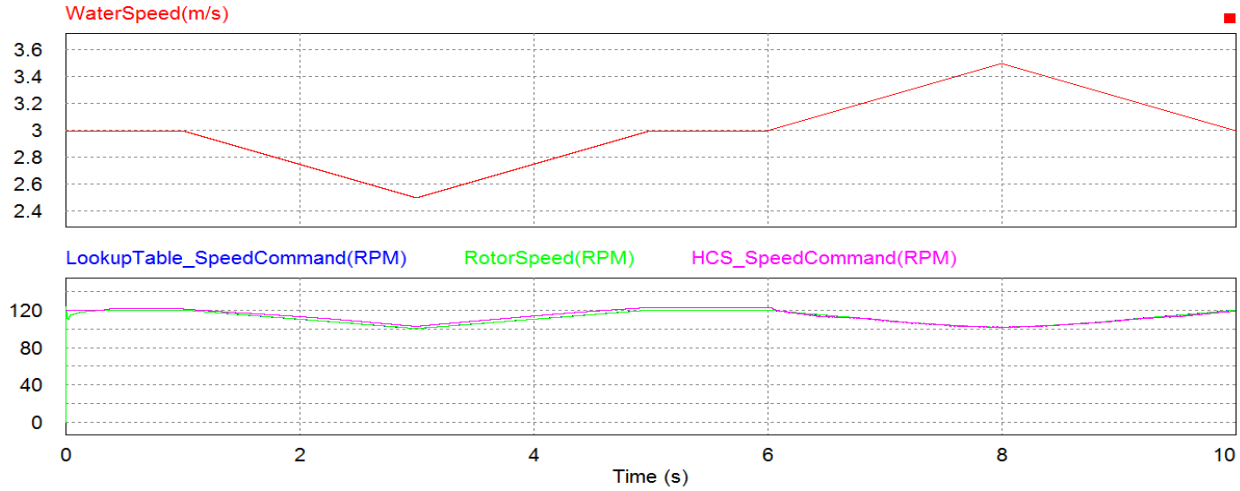

Figure 4-18 Water speed and speed commands of Case 3

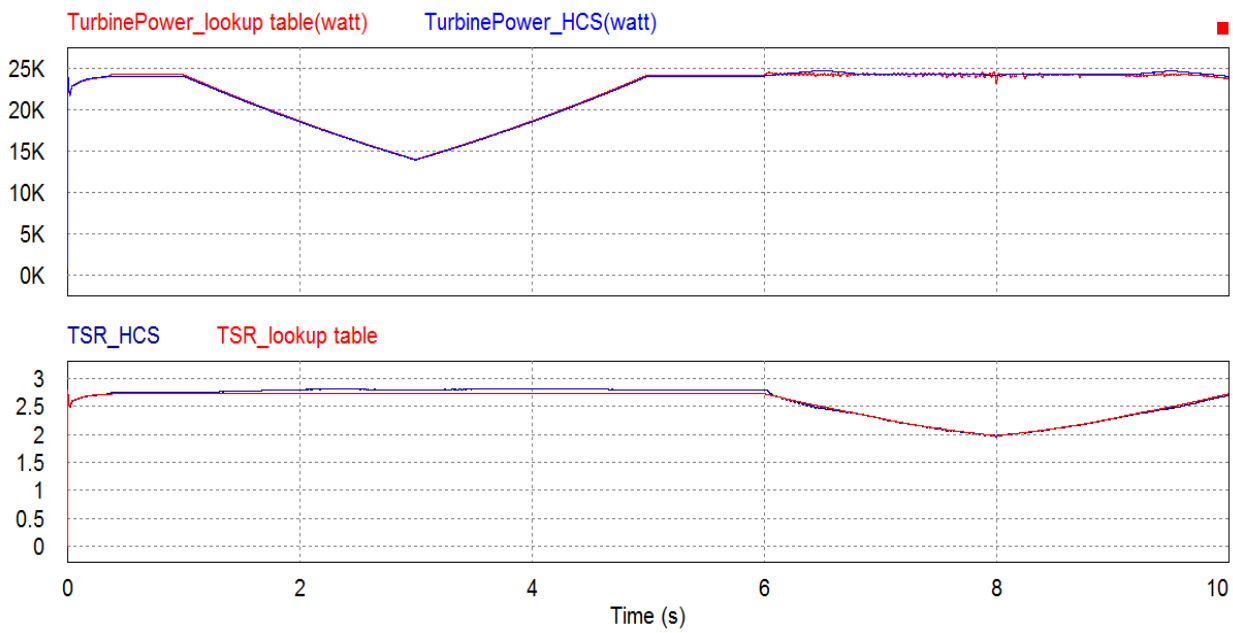

Figure 4-19 TSR and power outputs of Case 3

As it is shown, the water speed decreases from 3m/s to 2.5m/s at 1s, then goes back to 3m/s at 5s, goes up to 3.5m/s at 8s and return to 3m/s. The initial condition of the rotor speed is assumed to be the optimal rotational speed (120RPM) for the constant water speed 3m/s. When the water speed drops down to 2.5m/s, the hill-climb searching method detects the change in the turbine output power and reduces the reference speed from 120RPM to 100RPM to extract the maximum available power. When the water speed is higher than the rated water speed of 3m/s, the hydrokinetic system operates in the Power regulation region. As shown in figure 4-18, the speed command curve obtained from hill-climb searching method is close to the reference speed from the lookup table method. Figure 4-19 indicates that the turbine output power and TSR value are almost the same for these two methods. Even though a small error exists in the reference speed between these two methods, the error is negligible and does not have any impact on the power output. Therefore, when a fluctuation or eddies occurs in the constant water speed, the hydrokinetic system can manage to produce the available power with the function of MPPT and Power regulation.

4.7.4 Case 4 – Water speed in a sine wave form

Another case is given as the water speed being like a sine waveform, which represents a continuous fluctuation or eddies occurring in the river circumstance. Even though, this water

condition is rarely happened for river application, the hydrokinetic system should be able to operate satisfactory rather than turn off.

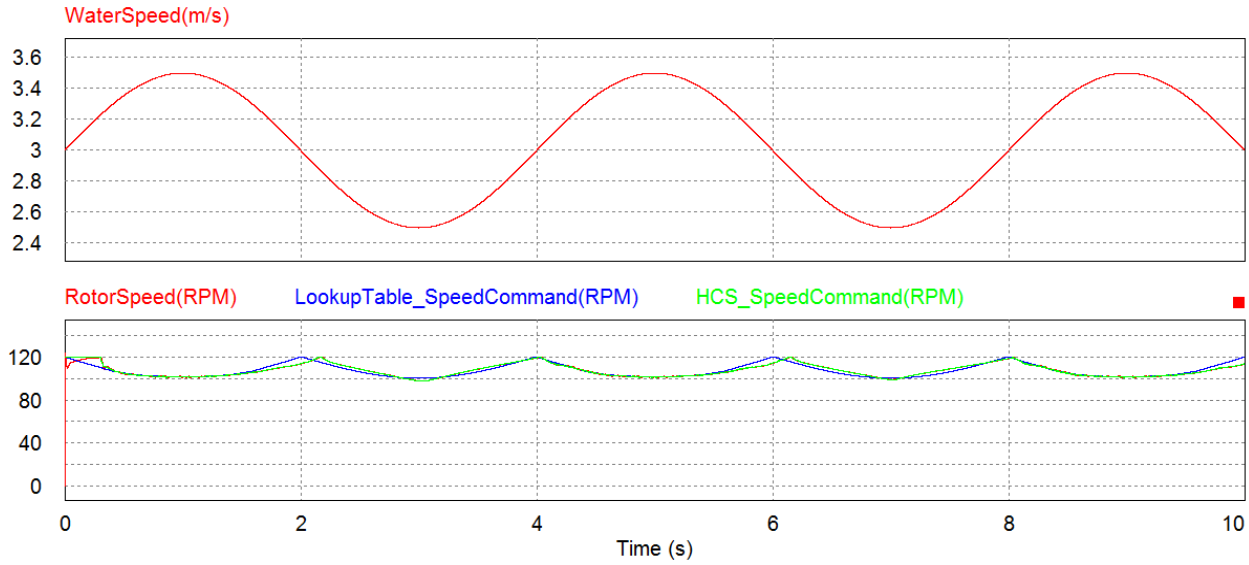

Figure 4-20 Water speed and speed commands of Case 4

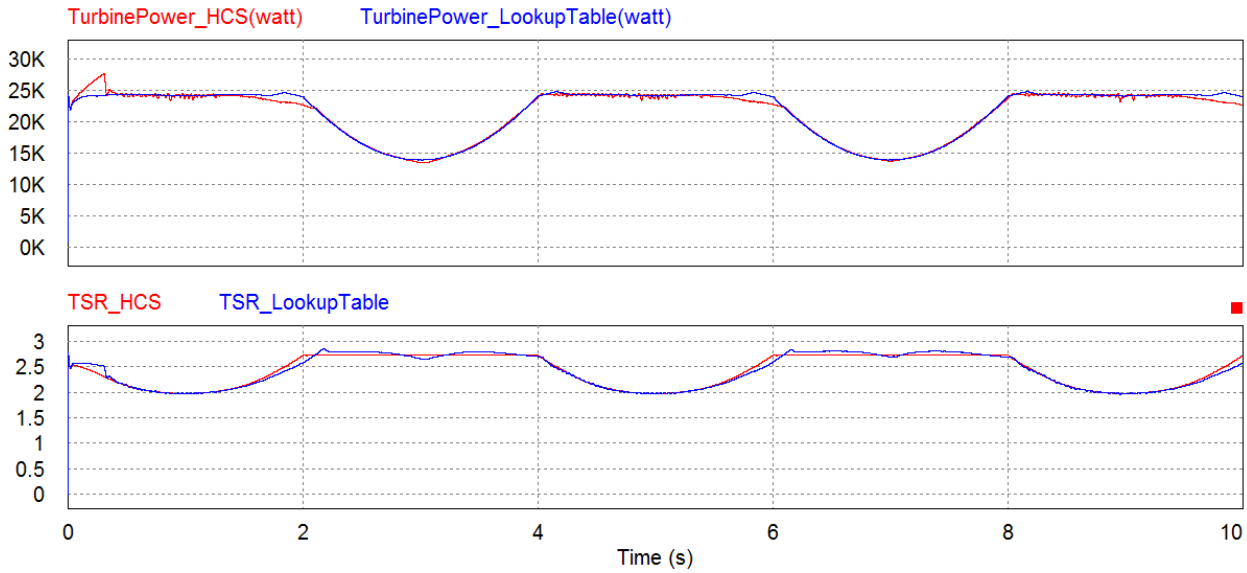

Figure 4-21 TSR and power outputs of Case 4

Figure 4-20 shows that the water speed curve varies between 2.5m/s and 3.5m/s as a sine wave. In order to avoid the starting transient problem, the initial speed of the turbine is set at the rated speed 120 RPM when the water speed is 3m/s. Because the water speed changes around 3m/s, the operation status changes between the MPPT region and the power regulation region alternatively. In this case, the results of lookup table method are used to compare with the results of hill-climb searching method. From the second plot of figure 4-20, the speed command from hill-climb searching method does not coincide to the one from lookup table method. This is

because the response time of the hill-climb searching method is not as fast as lookup table method when water speed is changing fast. When water speed information is loaded into the lookup table, a speed command can be output to the controller immediately, while for the hill climb searching method, calculation is required to get the same speed command. Even though there is an error in the rotor speed between the hill-climb searching method and lookup table method, the turbine output power curve and TSR curve from hill-climb searching method are close to the target values in figure 4-21. Because water condition does not always change sinusoidally, the requirement for the hydrokinetic system is to be able to deal with this situation with outputting reasonable power. However, if a dramatic variation is occurring on the water speed, the system should be shut down in order to prevent the system from unpredictable damage.

4.7.5 Case 5 – Water speed increases from 1.5m/s to 4.5m/s to 2.5m/s

As discussed in Chapter 3, 1.5m/s is the cut-in speed and 4.5m/s is the cut-off speed respectively. For this water condition, the hydrokinetic system should be operating at the MPPT region first and then with the water speed increasing the system will operates in the Power regulation region as the water speed increases. When the water speed decreases below the rated water speed (3m/s), the system should switch back to the MPPT region. The objective of this case is to demonstrate the feasibility of the hill-climb searching method over the whole operation period.

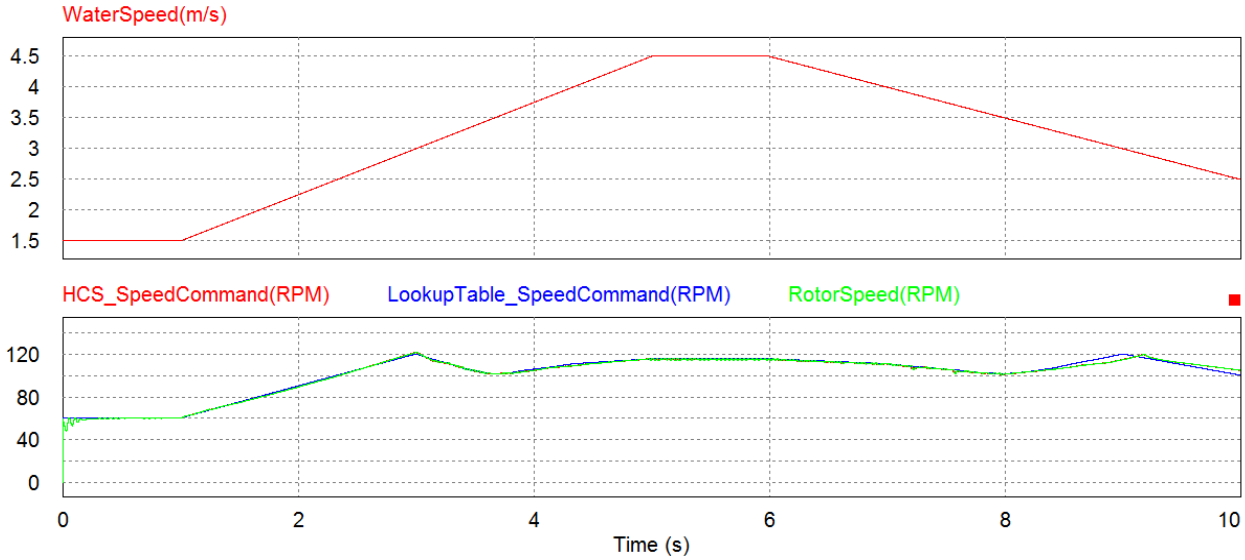

Figure 4-22 Water speed and speed commands of Case 5

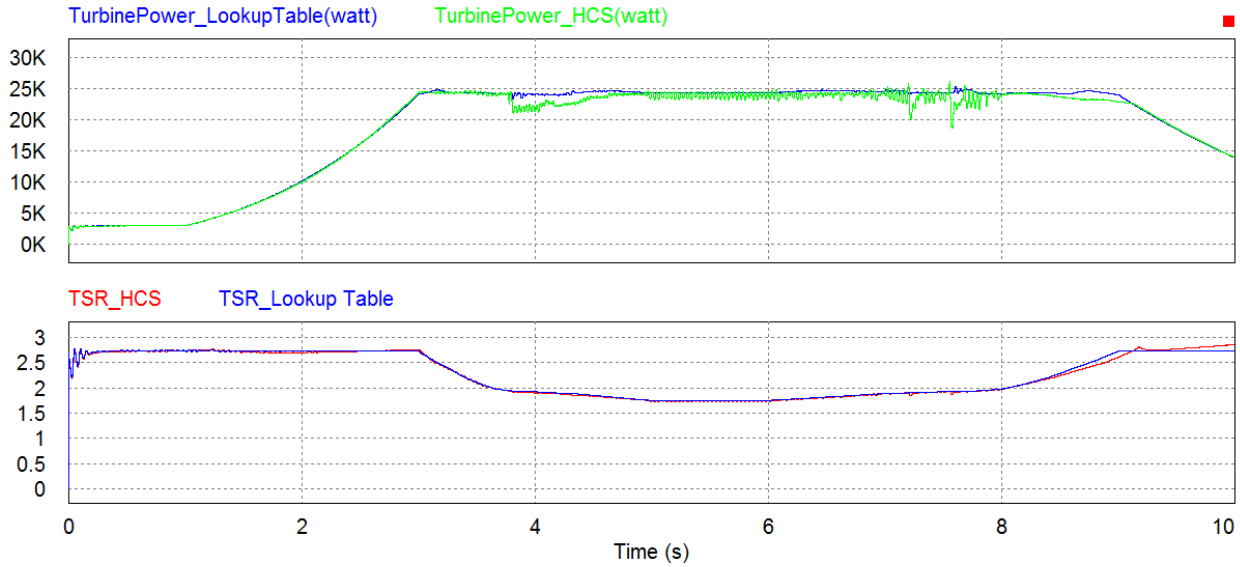

Figure 4-23 TSR and power outputs of Case 5

In this case, the results of lookup table method are used as the target to compare with the results of hill-climb searching method. In Figure 4-22, the whole period can be divided into 3 subparts. The first subpart is from 0s to 3s that the water speed increases from 1.5m/s to 3m/s. During this period, the hill-climb searching method operates to find the maximum output power and tries to maintain the TSR at optimal value 2.75. The second period starts at 3s and ends at 9s. Because the water speed is higher than the rated water speed, so the rotor speed should be reduced and the output power should be regulated and maintained at the maximum available power (24.2kW). For the last period, the water speed decreases continuously down to 2.5m/s, so the hill-climb searching method should look for the maximum power point again. As shown in figure 4-23, the output turbine power curve is close to the reference value during the whole period and also the TSR is close to the target value (2.75 for MPPT region and lower for PR region). Because the hill-climb searching method is not as precise as lookup table method, small errors may exist in the simulation results. As a result, it can be seen that with the help of hill-climb searching method, the hydrokinetic system is continuously operating at the optimal power point for each corresponding water speed and it can deal with different water situations stably and efficiently.

Chapter 5 – Conclusions and Future Work

This thesis presents the power converter and rotor speed controller design of the hydrokinetic system. The idea of designing this hydrokinetic system is based on the Mavi's hydrokinetic turbine project. The objective of this work is to extract the maximum available power by implementing MPPT and controlling the power converter and rotor speed controller for different water flowing conditions. In the thesis, each component of the hydrokinetic system has been described and analyzed based on their operation principles. For the design of the rotor speed controller, a number of control strategies are introduced and compared. As the result, the Field Oriented Control strategy, which is proved to be a robust and reliable method, is employed as the PMSG rotor speed control method. By using the PI controller tuning method—Modulus Optimum, the parameters of PI controllers can be calculated efficiently. For designing the power converter, the lookup table method and hill-climb searching method (coded in C) are purposed in the sensor-based system and sensor-less system respectively. As discussed in chapter 4, the lookup table method provides a straightforward, fast and reliable MPPT/Power regulation function, but this method requires a pretest for the characteristics of the corresponding turbines and also a water speed sensor to measure the water speed situation. The precision of the speed sensor determines the efficiency of the MPPT function, but the more precise sensor always costs more. The hill-climb searching method can look for the maximum power point by the observation and perturbation algorithm without knowing any characteristic information of different turbines. In addition, variable step change for the reference rotor speed can increase the efficiency and accuracy of locating the maximum power point, however, comparing with the lookup table method, the hill-climb searching method always spends longer time for searching the maximum power point when the water speed changes. Because the water current changes very slow for a long period and the switching frequency is high enough, the response time of hill-climb searching method is acceptable and good enough.

From the simulation cases in chapter 4, it can be seen that the results from the hill-climb searching method are close to the results from lookup table for some water conditions. The hill-climb searching method is realized in C code which means adjusting and optimizing the algorithm is easy. Therefore, as conclusion, the hill-climb searching method is better than its

lookup table alternative. In order to demonstrate the feasibility of the hydrokinetic system, a simulation model is built with the PSIM software and five different water condition cases are simulated. Eventually, the power converter and rotor speed controller can realize the MPPT/Power regulation function as expected, so the objective of this project is achieved, however, there are still some future work and issues needed to be resolved. Firstly, this paper presents the stand-alone system, and the power grid-connected system may be discussed in the future work. Secondly, because the system initial problems are technical difficulties, so the initial issues are assumed ideally and the real transient problems should be investigated in the hardware testing. Thirdly, due to some unpredictable reasons, only the stand-alone system has been built and tested. The test of connecting the VFD and PMSG is still in progress. The hardware testing results could be used to optimize and improve the MPPT/Power regulation algorithm.

In the end, it is my hope that this hydrokinetic system and its further developments can be used as an economically viable, environmentally friendly source of electricity on a commercial scale.

References

[1] L.I. Lago, F.L. Ponta and L. Chen, "Advances and Trends in Hydrokinetic Turbine System," Department of Mechanical Engineering - Engineering Mechanics, Michigan Technological University, Houghton, MI, 49931, USA, Energy for Sustainable Development, 14 (2010) 287-296

[2] World Energy Council, "*World Energy Resources-2013 Survey*," 2013

[3] J. Twidell and T. Weir, "*Renewable Energy Resource,"* Chapter 13, Taylor & Francis, 2006

[4] "Clean Energy—How Hydrokinetic Energy Works" by Union of Concerned Scientists, Accessed 26 April 2014, Available from http://www.ucsusa.org/clean_energy/our-energy-choices/renewable-energy/how-hydrokinetic-energy-works.html

[5] S. Khan, "Modeling and Performance Analysis of a Direct-Driven PMSG for Variable Speed Wind Energy Conversion System," Purdue University, Hammond Indiana, Dec 2012

[6] CEATI International, 2009 "Variable Frequency Drives Energy Efficiency Reference Guide".

[7] A. Grauers, "Efficiency of three wind energy generator systems," *IEEE Trans. Energy Convers*, vol. 11, no. 3, pp. 650–657, Sep. 1996

[8] A. Kilk, "Low-Speed Permanent Magnet Synchronous Generator for Small-Scale Wind Power Application," Oil Shale, Vol. 24, No. 2 Special, pp 318-331, 2007

[9] Simulating Permanent Magnet Generators from COMSOL, Accessed 17 June 2014, Available from: http://www.comsol.com/blogs/simulating-permanent-magnet-generators

[10] P.M. Anderson and A.A. Fouad, "*Power System Control and Stability*," Piscataway, N.J.: IEEE Press; Wiley-Interscience, 2003.

[11] J. Lepka and P. Stekl, "3-Phase AC Induction Motor Vector Control Using a 56F80x, 56F8100 or 56F8300 Device, Design of Motor Control Application," an application note, AN1930 Rev.2, 2/2005, Free-scale Semiconductor Inc., 2005

[12] M. Chinchilla, S. Arnaltes, and J.C. Burgos, "Control of Permanent-Magnet Generators Applied to Variable-Speed Wind-Energy Systems Connected to the Grid," *IEEE Transactions on Energy Conversion*, vol 21, No. 1, March 2006

[13] C. E. A. Silva, R. T. Bascope and D. S. Oliveria Jr., "Three-Phase Power Factor Correction Rectifier Applied to Wind Energy Conversion System," *Applied Power Electronics Conference and Exposition 2008*, APEC 2008, pp. 768 – 773, Feb 2008.

[14] P. Luukkonen, P. Bateman1, J. Hiscock, Y. Poissant, D. Howard and L. Dignard-Bailey, "National Survey Report of PV Power Applications in Canada 2012," CanSIC–national trade association, June 2013

[15] VACON "Vacon NX P user Manual," 2013

[16] T. J. Hall, "Numerical Simulation of a Cross Flow Marine Hydrokinetic Turbine," Master thesis, Department of Mechanical Engineering, University of Washington, 2012

[17] J. Khan, "State of River Energy technology: In-stream hydrokinetic turbines," Powertech Labs, British Columbia, Canada. 2006.

[18] Cristian Busca, Ana-Irina Stan, Tiberiu Stanciu and Daniel Ioan Stroe, "Control of Permanent Magnet Synchronous Generator for Large Wind Turbines," *IEEE*, Department of Energy Technology Aalborg University, Denmark 2010

[19] Andréa Cimpoeru, "Encoderless vector control of PMSG for wind power applications," Master thesis, Departament of Energy Tehnology-Pontoppidanstræde 101 Aalborg University, Denmark 2010

[20] G. Kohlrusz and D. Fodor, "Comparison of scalar and vector control strategies of induction motors," University of Pannonia, Faculty of Engineering, Insititude of Mechanical Engineering, Automotive System Engineering Group, H-8200, Veszprem, Egyetem str. 10., Hungary

[21] E. Morris, D. Armitage "Choosing a motor control platform and drive system," *A Guide to Standard Medium Voltage Variabe Speed Drive*, Part 2, ABB Swizerland Ltd..

[22] S. Chi and L. Xu, "Development of sensorless vector control for a PMSM running up to 60,000 rpm,*" In IEEE International Conference on Electric Machines and Drives*, pages 834-839, May 2005.

[23] Christian Busca,"Open Loop Low Speed Control for PMSM in High Dynamic Applications,*"* Master thesis, Departament of Energy Tehnology-Pontoppidanstræde 101 Aalborg University, Denmark 2010
[24] N. Freire, J. Estima, A. Cardoso "*A Comparative Analysis of PMSG Drives Based on Vector Control and Direct Control Techniques for Wind Turbine Applications*," University of Coimbra, University of Beira Interior, Instituto de Telecomunica ções.
[25] S. V. Paturca, M. Covrig, and L. Melcescu, "Direct Torque Control of Permanent Magnet Synchronous Motor (PMSM) - An approach by using space vector modulation (svm)," *Int. conference on Electric power systems*, Tenerife, Spain, p. 6, 2006.
[26] M. Roman, "*Modification of Symmetric Optimum Method*," ASR '2005 Seminar, Instruments and Control, Ostrava, April 29, 2005
[27] Gene F. Franklin, J.D. Powell, A. Emami-Naeini, *Feedback Control of Dynamic Systems*, Fifth Edition, Prentice Hall, USA, 2006, ISBN 0-13-149930-0.
[28] G. D. Moor and H. J. Beukes, "Maximum Power Point Trackers for wind turbines," *35th annual IEEE Power Electronics Specialists Conference*, Aachen Germany 2004
[29] E. Koutroulis and K. Kalaitzakis, "Design of a Maximum Power Tracking System for Wind Energy Conversion Applications," *IEEE Transactions on Industrial Electronics*, Vol. 53, # 2, April 2006.
[30] G. Putrus, M. Narayana, M. Jovanovic and P. S. Leung, "Maximum power point tracking for variable-speed fixed-pitch small wind turbines," *20th International Conference on Electricity Distribution*, Prague, 8-11 June 2009
[31] R. Datta and V.T. Ranganathan, "A Method of Tracking the Peak Power Points for a Variable Speed Wind Energy Conversion System," *IEEE Transaction On Energy Conversion*, VOL. 18, # 1, March 2003
[32] Q. Wang and L. Chang, "An Intelligent Maximum Power Extraction Algorithm for Inverter–base Variable Speed Wind Turbine Systems," *IEEE Transaction on Power Electronics*, VOL. 19, #5, September 2004
[33] Robert C. Reuter and Mark H. Worstell, "Torque Ripple on Vertical Axis Wind Turbine," Sandia Report by Sandia National Laboratories, SAND78-0577, 1978
[34] M.J. Khan, M.T. Iqbal and J.E. Quaicoe, "Dynamics of a vertical axis hydrokinetic energy conversion system with a rectifier coupled multi-pole permanent magnet generator," The Institution of Engineering and Technology, IET Renew. Power Gener, 2010, Vol. 4, Iss. 2, pp. 116–127, 2010
[35] d-q-0 transform by Open electrical, Accessed 25 may 2014, Available from: http://www.openelectrical.org/wiki/index.php?title=Dq0_Transform

Appendices

Appendix A: Datasheet of Selected PMSG

	Rated speed	Rpm	80
Rated power at rated speed	Rated power	W	15029
	Input torque at rated speed	N.m	2196
	Efficiency at rated power	%	82
	Current at rated power	Amps	38.4
	Voltage at rated power	V	230
Rated power at half speed	Rated power at half speed	W	6026
	Input torque at half speed	N.m	2196
	Efficiency at half speed	%	68
	Number of poles (number of pole pairs)		48(24)
	Cogging torque	N.m	22
	Phase resistance at 20 ℃	Ohm	0.53
	Phase inductance	mH	6.3
	Voltage at no load (back emf) at 20 ℃	V	307
	Rotor inertia	$g.m^2$	5080
	Weight	Kg	138
	Power cable square section	mm^2	4*70
	Power cable diameter	mm	13.4

Appendix B: C code Used in the PSIM MPPT Block

```
#include <Stdlib.h>
#include <String.h>
#include <math.h>
#include <Psim.h>
// PLACE GLOBAL VARIABLES OR USER FUNCTIONS HERE...
double RPM=120;       // speed reference {RPM]
double RPM_inc=0;     // Speed set point increment [RPM]
double t_elapsed=0; // Time elapsed since last update [seconds]
double t_total=0; //time counter
double P_old=0;          // Old power [Watts]
double P=0;              // Current power [Watts]
double P_delta=0; // Change in power [Watts]
double a=0;//judgement value
double P_delta_old=0;
double delta=0; //power variation between P(k) and P(k-1)
double C_step =0.05; //step size factor
double P_store=3000; // temporary memory for power
double delta_old=0; //temporary memory for delta_p
double slope=0; // slope of current power variation
double slope_m=0.2; //adjusted slope value
double slope_old=0; // temporary memory for slope
double n=1; //counter
double slope_total=0; // parameter for slope optimization
double m=1;// counter
double slope_d=0; //slope of current power variation
double slope_total_d=0; //parameter for slope optimization
double slope_old_d=0;//temporary memory for slope
//////////////////////////////////////////////////////////////////////
// FUNCTION: SimulationStep
//   This function runs at every time step.
//double t: (read only) time
//double delt: (read only) time step as in Simulation control
//double *in: (read only) zero based array of input values. in[0] is the first node, in[1] second input...
//double *out: (write only) zero based array of output values. out[0] is the first node, out[1] second output...
//int *pnError: (write only)  assign  *pnError = 1;  if there is an error and set the error message in szErrorMsg
//    strcpy(szErrorMsg, "Error message here...");
// DO NOT CHANGE THE NAME OR PARAMETERS OF THIS FUNCTION
void SimulationStep(
                              double t, double delt, double *in, double *out,
                               int *pnError, char * szErrorMsg,
                               void ** reserved_UserData, int reserved_ThreadIndex, void * reserved_AppPtr)
{
P=in[0];   //input turbine power
P_old=P_store;   //turbine power of last time step
delta=P-P_old;    //power change deltaP
P_store=P;
out[1]=P_old;
out[3]=delta;
t_total+=delt;
if (t_total<0.1)
{
out[0]=RPM; // reduce the effect of the power ripple at beginning
}
else
{
t_elapsed+=delt;
if (t_elapsed>0.005){
    if (P>=25500) // Power Regulation
              {            slope_total=0;
                            slope_old=0;
                            a=-2; // large size  step change to limit the turbine power
                            RPM_inc=a;
                            }
```

```
            else if(P>=24800&&P<25500)
                        {   slope_total=0;
                            slope_old=0;
                            a=-0.3; // small size step change
            RPM_inc=a;}
    else {     // MPPT
        if (delta>0.1) {
      // Change in power, change set point.
            if (a>=0.0) {
                        slope=(delta-delta_old)/0.005; // slope of power variation
                        if(abs(slope)>10)
                        {   slope=10;}
                            slope_total=abs(slope)+slope_old;
                            slope_m=slope_total/n;
                            n+=1;
                            slope_old=slope_total;
                            delta_old=delta;
                            a= C_step *abs(slope_m);
                            RPM_inc=a;
                    }
                            else {    slope_total=0;
                                      slope_old=0;n=1;
                                      a=-0.1;
                                      RPM_inc=a;  }
                    }
            if (delta>-0.1&& delta<0.1)
                        {
                        RPM_inc=0;  }
            if (delta<=-0.13) {
                            if (a>=0) {    slope_total=0;
                                           slope_old=0;
                                           n=1;
                                           slope_d=(delta-delta_old)/0.005; // slope of power variation for  decreasing water speed
                                           if(abs(slope_d)>10)
                                           {
                                           slope_d=10;}
                                           slope_total_d=abs(slope_d)+slope_old_d;
                                           slope_m=slope_total_d/m;
                                           m+=1;
                                           slope_old_d=slope_total_d;
                                           delta_old=delta;
                                           a= C_step *abs(slope_m);
                                           RPM_inc=-a;}
                            else {
                                           slope_total=0;
                                           slope_old=0;n=1;
                                           a=-0.22;
                                           RPM_inc=-a; }
            }
    }
    // hard speed limit
    if ((RPM+RPM_inc)>130)
     {
      RPM_inc = 130 - RPM;  }
    // clean up.
    RPM += RPM_inc;
    t_elapsed = 0;}
  out[0]=RPM;            // output speed reference
  out[2]=a;
  out[4]=slope_m;
}
}
```

Appendix C: VFD Block Diagram [15]

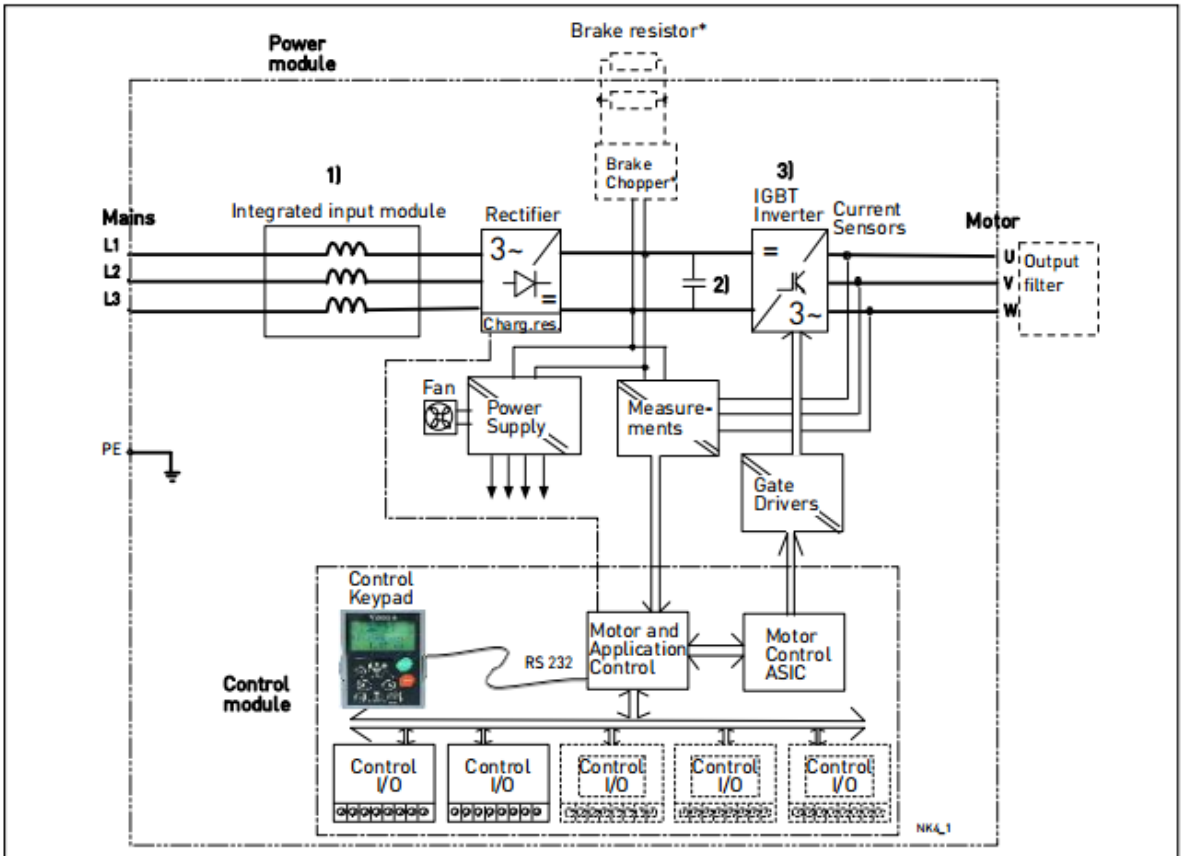

*The brake resistor can be installed internally in sizes FR4 to FR6 (NX_2 and NX_5). In all other frames of voltage classes NX_2 and NX_5, as well as in all frames of all other voltage classes, the brake resistor is available as option and installed externally.
Brake chopper belongs to the standard equipment in sizes FR4 to FR6, while in greater sizes (FR7 to FR9) it is optional.

Appendix D: Hydrokinetic System Model in PSIM